Characterization of the Conformational Probability of N-Acetyl-Phenylalanyl-NH_2 by RHF, DFT, and MP2 Computation and AIM Analyses, Confirmed by Jet-Cooled Infrared Data

Gregory A. Chass,*[†,‡,§,⊥,☆,◇] Reinard S. Mirasol,[†,‡,∥] David H. Setiadi,[†,‡] Ting-Hua Tang,[†,‡] Wutharath Chin,[§] Michel Mons,[§] Iliana Dimicoli,[§] Jean-Pierre Dognon,[§] Bela Viskolcz,[∥] Sándor Lovas,[⊥] Botond Penke,[#,★] and Imre G. Csizmadia[†,‡,#]

Global Institute of COmputational Molecular and Materials Science (GIOCOMMS), 2-158 Major Street, Toronto, Ontario M5S 2K2, Canada, Lash Miller Chemical Laboratories, Department of Chemistry, University of Toronto, 80 St. George Street, Toronto, Ontario M5G 2E8, Canada, Laboratoire Francis Perrin (URA CNRS 2453), Service des Photons, Atomes et Molécules, and CEA / DSM / DRECAM, Centre d'Etudes de Saclay, Bât. 522, 91191 Gif-sur-Yvette Cedex, France, Department of Chemistry, Juhasz Gyula Teaching College, University of Szeged, Szeged 6725, Hungary, Department of Biomedical Sciences, School of Medicine, Creighton University, 2500 California Plaza, Omaha, Nebraska 68178, Department of Medical Chemistry, University of Szeged, Dóm tér 8, H-6720 Szeged, Hungary, Protein Chemistry Research Group, Hungarian Academy of Sciences, University of Szeged, Dóm tér 8, H-6720 Szeged, Hungary, Instituto de Biocomputación y Física de Sistemas Complejos (BIFI), Corona de Aragón 42, 50009 Zaragoza, Spain, and Zymeworks Inc., Suite 201, 1401 West Broadway, Vancouver, British Columbia V6H 1H6, Canada

Received: November 15, 2004

Computational and experimental determinations were carried out in parallel on the conformational probability of N-Acetyl-Phenylalanine-NH_2 (NAPA). Ab initio computations were completed at the BLYP/6-311G(df,p), B3LYP/6-31G(d), B3LYP/6-31G(d,p), and B3LYP/6-31+G(d) levels of theory, labeled L/61fp, B/6, B/6p, and B/6+, respectively. Three experimentally identified conformers were compared with theoretical data, confirming their identities as the β_L^{anti}, $\gamma_L^{gauche+}$, and $\gamma_L^{gauche-}$ ($BACKBONE^{SIDECHAIN}$) conformers. Evidence comes from matching experimental and theoretical data for all three constituent N−H stretches of NAPA, with a $\Delta_{Experimental-Theoretical} = \sim 1-3\ cm^{-1}$, $\sim 0-5\ cm^{-1}$, and $\sim 1-6\ cm^{-1}$, at the L/61fp and B/6+ levels, respectively. Corrected-ZPE relative energies were computed to be 0.14, 0.00, 0.26 and 0.00, 0.67, 0.57 (kcal*mol^{-1}) for the β_L^{anti}, $\gamma_L^{gauche+}$, and $\gamma_L^{gauche-}$ conformers, respectively, at the L/61fp and B/6+ levels, respectively. The MP2/6-31+G(d) level of theory was subsequently found to give similar relative energies. Characterization of the intramolecular interactions responsible for red and blue shifting of the N−H stretches showed the existence of the following intramolecular interactions: $C{=}O_{[i]}\text{- - -}HN_{[i]}$, $(Ar_{[i]})\text{-}C_{\gamma}\text{- - -}HN_{[i+1]}$, $(Ar_{[i]})\text{-}C_{\delta}\text{-H- - -}O{=}C_{[i-1]}$ for β_L^{anti}; $C{=}O_{[i-1]}\text{- - -}HN_{[i+1]}$, $(Ar_{[i]})\text{-}C_{\gamma}\text{- - -}HN_{[i+1]}$, $(Ar_{[i]})\text{-C−H- - -}O{=}C_{[i]}$ for $\gamma_L^{gauche+}$; and $C{=}O_{[i-1]}\text{- - -}HN_{[i+1]}$ for $\gamma_L^{gauche-}$. Each of these interactions were further investigated and subsequently characterized by orbital population and Atoms-In-Molecules (AIM) analyses, with the identity of overlap and bond critical points (BCP) serving as 'scoring criteria', respectively. Experimental and theoretical carbonyl stretches were also compared and showed good agreement, adding further strength to the synergy between experiment and theory.

1. Introduction

Protein folding has become a central challenge to many disciplines, including the biomedical sciences, biology, biochemistry, chemistry, molecular physics, mathematics, informatics, and computer science.

The underlying mechanisms of protein folding may first be tackled through the characterization of the folding of short-peptides, with the latter as a prelude to the former.[1−3] Two approaches exist, specifically a holistic global, or macromolecular, one and a reductionist localized micromolecular alternative.[1,2] Precise and accurate characterization, using several methods, will allow for a complete understanding at the molecular level of the conformational preferences of individual amino acids in larger peptide models.

The setting up of a standardized and numerical definition of molecular structure, nondependent upon visualization[3,4] allows for a central data set to be engineered, constructed, and compiled. This is able to be used by all disciplines finding usefulness in the characterization and management of 'applicable' data sets (i.e. data warehousing, networking, and storage).

Through the investigation of molecular conformational probability distributions, one may be able to understand the bases of stability and the reason for the 'intermittent' or instantaneous 'poses' (conformations) the molecule adopts.[5−10] The forces stabilizing the molecule and allowing/disallowing the change

* Corresponding author e-mail: gchass@giocomms.org.
† Global Institute of COmputational Molecular and Materials Science (GIOCOMMS).
‡ University of Toronto.
§ Laboratoire Francis Perrin.
∥ Department of Chemistry, University of Szeged.
⊥ Creighton University.
Department of Medical Chemistry, University of Szeged.
★ Hungarian Academy of Sciences, University of Szeged.
☆ Instituto de Biocomputación y Física de Sistemas Complejos (BIFI).
◇ Zymeworks Inc.

10.1021/jp040720i CCC: $30.25 © 2005 American Chemical Society
Published on Web 05/27/2005

from one conformational 'pose' to another (conformational change) are tied into the bases of the interactions themselves. Stable structural poses (conformations) represent structural manifestations of an 'energetic agreement' between all degrees of freedom.[5,11−12]

All degrees of freedom must, therefore, be accurately characterized to quantitatively evaluate their separate energetic contributions to the total energy of a structure; known as energetic partitioning.[5,10,11,13] Energetic partitioning can only be performed accurately and precisely (i.e. repeatable), if and only if all 3N-6 degrees of intramolecular freedom are included into an analytical expression. This analytic formalism may then be used to uncover and to quantitatively characterize the coupling between all of these 3N-6 degrees of freedom.

A proper and complete examination of the normal modes of molecular vibration (stretches, bends, wags, rocks, rotations, scissoring, etc.) can be used to evaluate the magnitude of coupling between the degrees of freedom and may be performed using theoretical quantum chemical computations in joint with experimental Infrared (IR) examinations.[11]

The degree of red and blue shifting of theoretically and experimentally determined absorption bands is attributed to structural properties and intramolecular interactions. Differing structures, isomers, enantiomers, and even conformers provide nonequivalent environs for each normal mode, effecting an activation or deactivation of nuclear vibration. Those vibrational modes' movements that are facilitated or restricted require higher or lower energy, respectively, to activate.

For example, the fully extended beta-backbone conformation, β_L (φ_i, $\psi_i \equiv$ *anti* $\equiv +120° \leftrightarrow +240°$), restricts the normal modes involving the carbonyl oxygen and amidic-hydrogen forming a hydrogen bond (H-bond) (i.e. C═O and N−H stretches) effecting a higher energy to activate. The elevated energetic requirement may be observed as a blueshift in the absorption band of the affected normal modes.

These red and blue shifted absorption bands constitute the basis of conformational assignment from experimental IR data. Working with the red and blue shifting of these peaks, one can work a solution into the basis for these shifts—due to interactions with those moieties making the stretch either more or less 'energetically costly' to activate/animate. It is expected that the results from this theoretical study on Ac-Phe-NH_2 (NAPA) will aid in the experimental and theoretical assignment of peaks for di- and tripeptide systems containing phenylalanine.

The IR experiments must be highly deconvoluted and precise enough, where working on cooled species, with a conformational selection carried out using UV spectroscopy (double resonance IR/UV spectroscopy) to allow for structural settling into the minima on the PEHS. This affords high resolution, facilitating the end goal of characterizing each peak. Clearly the gas phase is the best choice for quantitative characterization of the qualitatively proposed experimental hypotheses and expectation.

With a joint experimental and theoretical characterization of the normal modes one may accurately quantify energetic topologies (Potential Energy Curves, Surfaces and Hypersurfaces, PEC, PES, and PEHS, respectively) and Morse potentials. From the Morse potentials, one can then reparametrize force fields not only based on molecular constitution (i.e. peptide primary structure) but also on conformation and its probability distribution. This sort of mathematical amelioration of force field codes is currently ongoing and will improve the existing and related molecular mechanics (MM) and molecular dynamics (MD) studies,[14−16] specific to each peptide residue, one of the long-term goals of this work.

CHART 1

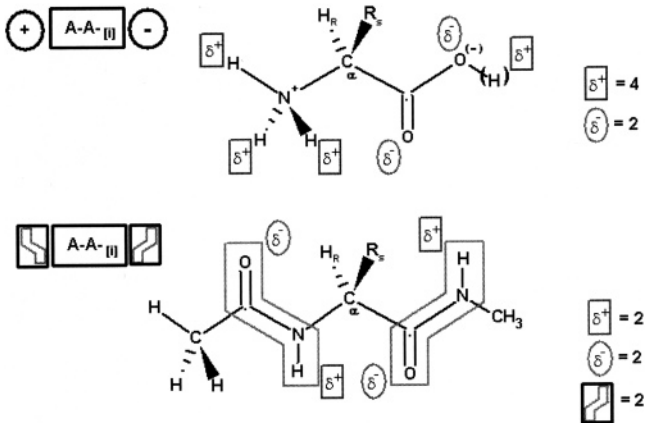

Free amino acid models are not appropriate for modeling peptide folding,[17] since the free amino acid model allows for stabilizing or destabilizing forces to be included that are not valid for peptides.[17] Chart 1 shows how this is possible for an amino acid (labeled i); here the relatively acidic and highly polar C-terminal carboxyl hydroxyl group (−COOH) allows for intramolecular interactions (whether of H-bond, van der Waals (vdW) or London and Dispersion character) which may be either stabilizing or destabilizing in nature.

The N- and C-terminally protected amino acid diamide, as a dipeptide model, is able to model the inductive (through bond) and field (through space) energetic and electronic density contributions of neighboring peptide residues. As can be seen on the right side of Chart 1, the free amino acid model neither includes these neighboring influences nor does it properly provide the electrostatic environment of the peptide group.

Intramolecular ring formation, via hydrogen bonding, is discussed in further detail in section 4.4.1; however, it is stated here that the β_L, γ_L, and γ_D conformers form 5-, 7- and 7-membered rings, respectively. These conformers are sometimes named according to their intramolecular rings, specifically C_5, C_7^{ax} (ax = axial), and C_7^{eq} (eq = equatorial), for the β_L, γ_L, and γ_D structures, respectively; axial and equatorial are in reference to the position of the C_β (atom #13 in this model) relative to the intramolecular ring formed.

The β_L backbone conformation provides the required geometry for a $C{=}O_{[i]}$- - -$HN_{[i]}$ interaction (also known as the C_5 conformation) to occur, where a gamma backbone conformation (γ_L, γ_D) allows for a $C{=}O_{[i-1]}$- - -$HN_{[i+1]}$ stabilizing interaction (C_7^{ax}, C_7^{eq}, respectively). Free amino acid models do not allow for the latter type of intramolecular stabilization to occur, as they lack the $C{=}O_{[i-1]}$ and $HN_{[i+1]}$ groups.

The Ac-Phe-NH_2 system was chosen in this work to allow for both symmetric and antisymmetric C-terminal amine N−H stretches to be collected experimentally. The focus of this work favors the formulation of a theoretical-experimental synergy, therefore using the $-NH_2$ terminus, over the use of the more structurally accurate *N*-methylamide (NH−CH_3) C-terminal protecting group. Future works could undertake the characterization of the differences and similarities of Ac-Phe-NH_2 and Ac-Phe-NH-CH_3.[18]

Weakly polar interactions have long been thought to be influential in both the conformational probabilities (preferences) of peptide models and the perturbation of PEHSs.[6−9,19−39] All interactions, particularly C═O- - -HN and Ar- - -HN (Chart 2), and even the possible C═O- - -HC and N- - -HN interactions, may in fact be directing, influential, and observable in selected experimental and theoretical undertakings.

CHART 2

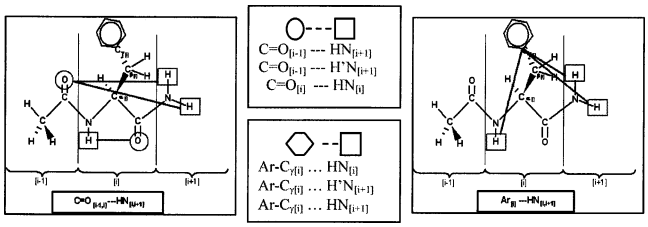

The possible C═O- - -HN and Ar−C_γ- - -HN interactions are diagrammatically depicted in Chart 2.

However, the quantitative characterization of the nature, identity, and energetic contribution of these interactions is a challenge to modern experimental and theoretical techniques and remains to be established. For example, a recent work's attempt to characterize the Ar- - -HN interaction was biased in its hypothesis that the interaction involves the centroid of the aromatic ring.[17] The centroid may be defined as the center of geometry, charge, or nucleophilicity (i.e. the specific atom or orbitals) involved in the donation of density to an amidic hydrogen.

It is proposed that matching of theoretical IR band signatures of Ac-Phe-NH_2 with experimentally determined bands will allow for a more complete understanding of the conformational preference of Phe in peptides as well as further established synergy between theory and experiment.[40]

2. Computational Methods

The Gaussian 98 program package (G98)[41] was used for all computations in this work. The common convergence criteria of 3.0×10^{-4}, 4.5×10^{-4}, 1.2×10^{-3}, and 1.8×10^{-3} were used for the gradients of the Root Mean Square (RMS) Force, Maximum Force, RMS Displacement, and Maximum Displacement vectors, respectively.

To meet the 'design criteria' for scalable *ab initio* biological 'building block' studies, a modular construct was employed that allowed for addition and/or removal of any portion of the model, without gross perturbation to the remainder.[3,40−41] The systematic construction of the Ac-Phe-NH_2 peptide model using precomputed molecular moiety 'modules' also benefited from the use of precomputed data. In turn, the constituent and 'total' Ac-Phe-NH_2 module will itself be able to be used in subsequent studies of larger and more complex (di-, tri-, oligo-) peptide systems containing Phe.[18] Although all assemblies of precomputed 'building blocks' must still be geometry optimized, the use of preoptimized portions allows for an overall increase in computational efficiency as well as theoretical accuracy and precision.[18,42] Figure 1 shows the modular nature of the model.

Unix-shell and *Practical Extraction and Report Language* (PERL)[43] scripts were developed and employed in order to increase efficiency of data and networking management. Computations were performed on highly available and distributed algorithm-specific hardware architectures to achieve fast, efficient, and highly organized results, housed in a growing database of computed structures,[3,4] easily accessed, and reused for related works. This and other ongoing computational studies were designed in preparation of processing vast amounts of data and allowing On-Line Analytical Processing (OLAP) manipulation, subsequent tabulation, and analysis of results.[43]

All atoms were numbered (Figure 1) and input structures constructed in accordance with an established standardized, numeric, and explicit methodology.[3,4] Each structure was initially geometry optimized using the *ab initio*[44] Restricted

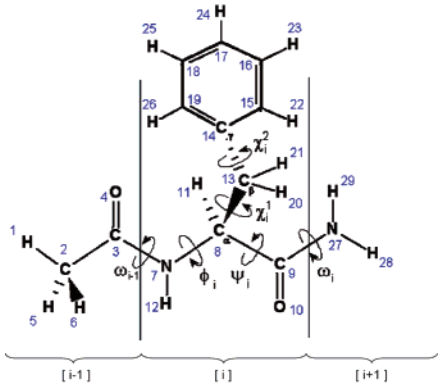

Figure 1. Representation of an established standardized numbering system of constituent atomic nuclei. Modular nature assigns a number to each atom of N-Ac-Phe-NH_2 (NAPA) consecutively from the N-terminus (left-most [i-1] module) through the central Phe (central [i] module) to C-terminal NH_2 protecting group (right-most [i+1] module). The 6 most structurally influential dihedral angles are shown (curved arrows) with their symbolic labels.

Hartree−Fock (RHF)[45] method, employing the split-valence 3-21G basis set.[46−48] Multi-Dimensional Conformational Analysis (MDCA)[49] was used to define the scope for the exhaustive conformational search, as the topologically possible set of conformers dictated by a grid-defined set of catchment regions. The large number of conformers is necessary to accurately characterize the topologically probable (stable) set of conformers emerging from the topologically possible set.[1−4,17,18,40,42,50−54] Conformational nomenclature follows the rules outlined in the literature.[1−4,17,18,40,50−54]

The χ_i^2 side chain dihedral angle (phenyl ring rotor) was modeled in the *gauche*$^+$ *(g*$^+$*)*, *anti (a)*, and *gauche*$^-$ *(g*$^-$*)* conformations. However, the g^+ and g^- rotamers have been shown to be stable and degenerate;[17] only the g^+ conformers are reported in this work.

The RHF/3-21G geometry optimized structural parameters were used as input in a subsequent theoretical refinement step, achieved using the more mathematically complete 6-31G(d) basis set. The RHF/6-31G(d) results were further refined through the inclusion of electron correlation effects at the BLYP/6-311G-(df,p) level, having been established as reliable for reproducing vibrational frequencies[55] and labeled L/6fp. The B3LYP method[56−58] was also used for comparison with other works, employing the split-valence 6-31G(d), 6-31G(d,p), and 6-31+G-(d) levels of theory,[46−48] labeled B/6, B/6p, and B/6+, respectively. Any conformer leaving its MDCA-defined catchment region at the lower RHF/3-21G level, its ideal MDCA-defined structure was reattempted at the RHF/6-31G(d) level and if necessary at any of the L/6fp, B/6, B/6p, and B/6+ levels. Of the RHF and B3LYP methods, only the L/6fp and B/6+ computed results are reported in this work; the B/6 and B/6p results are reported as Supporting Information.

Each stable conformer was subjected to frequency calculations in order to confirm their identity as being at true minima. The results also provided Zero Point Energy (ZPE) values, which were scaled by using a correction factor of 0.967[59] and added to the total energy of each conformer to provide more accurate energetic characterization of the conformers as well as the frequency of each of the normal modes. Frequencies were scaled by factors of 0.9600 as 0.9800, for higher and lower frequencies, respectively.[59]

Orbital populations and wave function-outputs were generated from the B3LYP/6-31G(d,p) optimized structures. Atoms-In-Molecules (AIM)[60] analysis was employed on the wave func-

tion-outputs. Bond Critical Points (BCPs), Ring Critical Points (RCPs), and Cage Critical Points (CCPs) were identified, and their positions were located for the $\beta_L{}^a$, $\gamma_L{}^{g+}$, and $\gamma_L{}^{g-}$ conformers. In the present work, BCP properties were obtained using the AIMPAC[61] and AIM98PC[62] program packages. The molecular graphs (AIM diagrams) presented were calculated and plotted using the AIM2000[63] program.

Structural variables of the $\beta_L{}^a$, $\gamma_L{}^{g+}$, and $\gamma_L{}^{g-}$ conformers, emerging from the stable B3LYP/6-31+G(d) geometry optimized set, were used as input files for geometry optimizations using the Møller−Plesset second-order (MP2) method,[64] in combination with the 6-31+G(d) basis set. This level of theory is labeled M/6+. This refinement employing perturbation theory was applied to Acetyl-Glycyl-amide (Ac-Gly-NH_2) and Acetyl-Alanyl-amide (Ac-Ala-NH_2), to uncover the basis of stability in NAPA. Specifically to increase understanding of the energetic contributions from the side chain and the intramolecular interactions involving the aromatic ring of Phe.

All molecular visualizations were constructed using the Molekel program package,[65,66] including structures and orbital population surfaces; the latter were constructed using a 0.098 cutoff value,[67] a fraction of the maximum physical extent of the electronic population distribution. Interpolated grid points with a value equal to this cutoff are considered to be the surface (points with a greater value are within the surface, lesser are without). The choice of cutoff is generally arbitrary; if it were too small the orbitals would engulf the molecule and little information could be discerned; if it were too high, then important features of the electron distribution (such as continuity over multiple atoms) might not be seen.[68−71]

All experimental IR results were obtained from the accompanying work.[72]

3. Results and Discussion

A qualitative proposal is made as to the foundations of the driving forces responsible for the conformational preferences of NAPA and other model peptide systems. The results are reported as backbone conformations following established conformational nomenclature.[3,4,6,13]

In total, 34 and 32 conformational minima, of the 81 MDCA-predicted and attempted, were found and confirmed by frequency analysis, for the L/61fp level and the B/6+ levels, respectively. Within the set of stable minima characterized, 17 and 16 were unique for the L/61fp and B/6+, respectively, with the $\chi_i{}^2$ torsion providing the degeneracy, as mentioned in the methods section. No stable ϵ_L backbone conformer was found. Figure 2 shows the approximate location of the B/6+ geometry optimized conformers on a traditional 'cut' (0° → 360°) of the Ramachandran map. Figure 3a,b shows the structure of the $\delta_L{}^{g+}$ and $\delta_L{}^{g-}$ BB conformers.

The three structures closest in agreement to experimental spectra[72] are displayed using visualization [Figure 4a−c].

3.1. Geometric Parameters and Structure. The optimized geometries for the structures at minima are listed in Table 1 and Supporting Information Table 1, displaying the results for the 6 most structural influential dihedral angles; specifically ω_{i-1}, φ_i, $\chi_i{}^1$, $\chi_i{}^2$, ψ_i, ω_i (Figure 1).

Two exceptions were found for the cross-level agreement of the topologically probable (stable) set of conformers, with $\beta_L{}^{g-}$ being unstable at the B/6+ level and converging to the $\gamma_L{}^{g-}$ conformer, despite repeated computational attempts to locate a stable minimum in the former catchment region. The same results emerged for the $\alpha_D{}^{g-}$ conformer, which continually converged to the $\gamma_L{}^{g-}$ conformer. These attempts follow the methods described in the literature.[17,40]

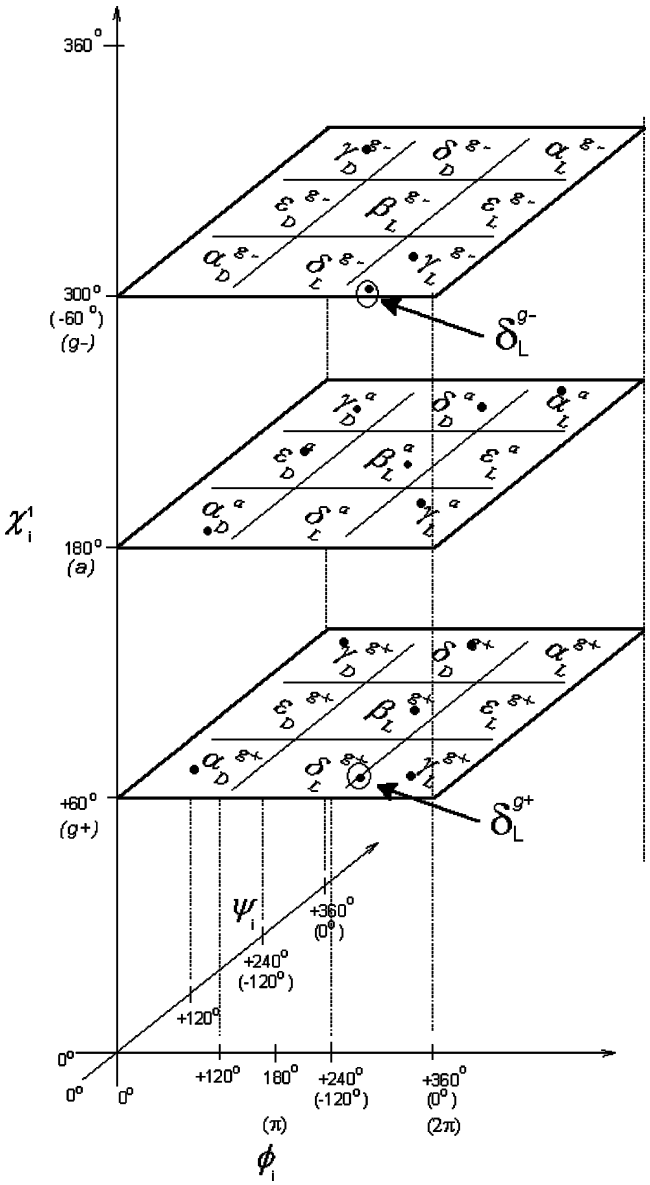

Figure 2. Traditional 'cut' (0° → 360°) of the Ramachandran map, showing the approximate location (dots) of stable backbone conformers, geometry optimized at the B3LYP/6-31+G(d) level of theory, for $\chi_i{}^1 \equiv g^+$ (*top*), $\chi_i{}^1 \equiv a$ (*middle*), for $\chi_i{}^1 \equiv g^-$(*bottom*). Backbone conformational nomenclature is 'labeled' in each catchment region. The two δ_L backbone conformers are circled to highlight the 'borderline' eclipsing geometries for their φ_i dihedral angle ($\varphi_i \cong +240°$).

The B/6+ geometry optimized results for the $\beta_L{}^{g-}$and $\alpha_D{}^{g-}$ conformers are reported as not found (N/F) in its respective place in Table 1. The 'missing conformers' at the 6-31+G(d) level of theory are attributed to a 'smoothening' of these regions of the potential energy hypersurface as a result of the inclusion of diffuse functions.

Despite being traditionally reported as being planar and rigid, the peptide bond displays some perturbation of this 'structural ideal'. The magnitude of this perturbation is on the order of 11.47°, 15.54°, 14.94°, and 13.01° for the ω_{i-1} dihedral of the $\delta_L{}^{g-}$ L/6fp, B/6, B/6p, and B/6+ conformers, respectively. The ω_i dihedral shows a maximum deviation from planarity of 8.48° for the $\delta_D{}^{g+}$ L/61fp conformer and 10.55°, 10.02°, and 9.22° for the $\delta_L{}^{g+}$ L/6fp, B/6, B/6p, and B/6+ conformers, respectively.

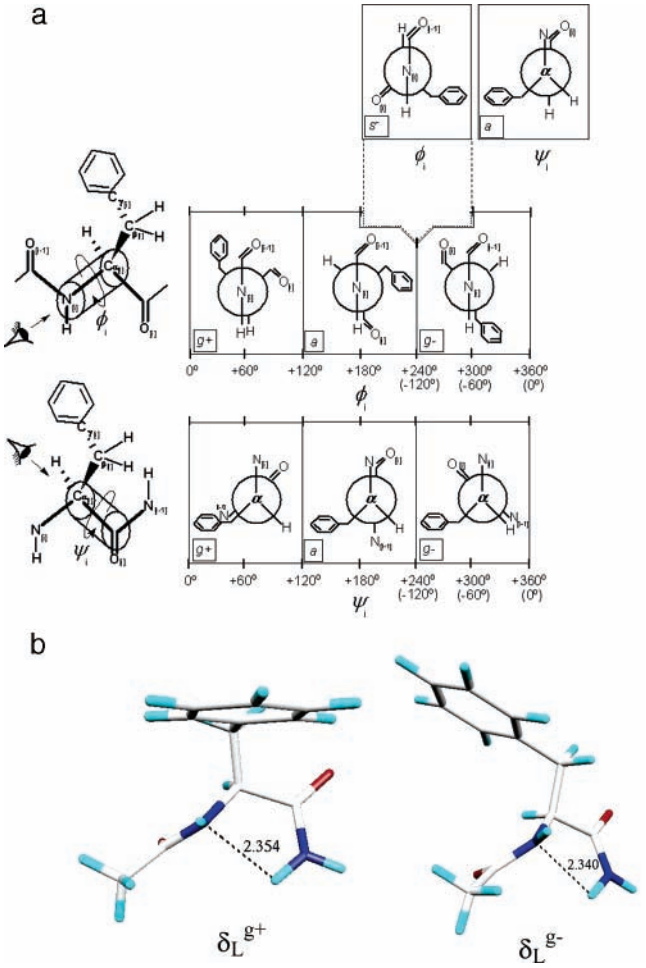

Figure 3. a. The resultant eclipsing φ_i rotor, where the C_α-H hydrogen and the $C{=}O_{[i-1]}$ oxygen are the eclipsing nuclei (*top right*). Despite being in an eclipsing conformation, the $\delta_L{}^{g+}$ conformer is relatively close in energy to the lowest energy conformer (see right-most column in Table B). Detailed Newman projections and viewing angles are also included for all MDCA-predicted rotamers of φ_i (*middle*) and ψ_i (*bottom*), for the g^+, *a*, *g* rotamers (*left, middle, right*), respectively. The eclipsing $\varphi_i \equiv +240°$ rotamer is fit relative to the three 'ideal poses' of the φ_i dihedral angle (dashed lines). b. Visual representations of the B3YLP/6-31+G(d) geometry optimized and frequency confirmed $\delta_L{}^{g+}$ (*left*) and $\delta_L{}^{g-}$ (*right*) conformers. The $N_{[i]}$- - -$HN_{[i+1]}$ interatomic distances (Å) are shown (dashed lines). These potential interactions form 5-membered intramolecular rings. Slight pyramidalization of the $N_{[i]}$ bond angles is apparent in both structures.

The origin of the nonplanarity in the ω dihedral angles is unknown at this point; however, there seems to be a relationship with the proximal bond angles and the degree of pyramidalization or planarity shown at the amidic $N_{[i]}$ and $C_{\alpha[i]}$, respectively. This phenomenon requires a separate study to determine its origin and influences upon structure.

Table 1 also shows that overall φ_i is structurally 'well behaved', whereas ψ is not. Furthermore, the φ_i dihedral adheres closely to the g^+ , *a*, and *g* 'sectioning' dictated by MDCA, with δ_L being the only exception with $\varphi_i = 120°$; Figure 3 shows this special eclipsing case for φ_i. STDEVs are also shown in Table 1 for the ω_{i-1}, $\chi_i{}^2$, and ωi dihedrals; $\chi_i{}^1$ was not subjected to this statistical treatment.

3.2. Total Energy, Zero-Point-Energy, and Relative Energy. Energetic results for total energy (Hartree), ZPE, and scaled-ZPE adjusted relative energy (kcal*mol^{-1}) are listed in Table 2.

Considering the scaled-ZPE adjusted relative energy, one finds that the $\gamma_L{}^{g+}$ conformer is the most stable (global minimum) for the L/61fp and B/6 and B/6p levels of theory. With the inclusion of diffuse functions, using the B/6+ level of theory, the $\beta_L{}^a$ structure is at the global minimum.

All BB conformers, with the exception of β_L, show an increase in relative energies with inclusion of corrected-ZPE. This is attributed to all NON− β_L BB conformers being in 'deep' minima and β_L being in a relatively flat part of the surface. The 'flat topology' of the β_L BB conformers are confirmed by these structures having low ZPE values.

The inclusion of diffuse functions has some influence on the relative energetic order of the conformers; a simple sketch of the molecular orbital (MO) overlaps expected between interacting atoms for each conformer is shown in Figure 5. The β_L conformer shows that the $C{=}O_{[i]}$ orbital must be evaluated further from the nucleus to have sufficient MO-overlap for effective sharing of the electron density. The MOs of the γ_L and γ_D conformers already have effective overlap between the orbitals, inherent to these geometries; this is displayed by their relatively close spatial proximities (Table 3).

Clearly Figure 5 is an extremely simplified and 'humanocentric' interpretation of the MO overlap but does show how the inclusion of diffuse and polarization functions perhaps aids to more significantly stabilize the beta-L conformer, in relation to the others. The $\beta_L{}^a$ B/6+ conformer is more stable than $\gamma_L{}^{g+}$, although not by a significant amount (∼0.6 kcal*mol^{-1} each). This 'β-lowering' is observed for the L/61fp, B/6p, and B/6+ levels. The qualitative analysis in Figure 5 also brings up the notion that a second diffuse function should be applied to all peptide model computations, as diffusivity, when applied to H atom, would be quite an important contributor to stability.

Classically, smaller rings are predicted as being more stable and thus one would expect the β_L structure to have a higher stability than the γ_L conformer.

The δ_L conformer 'defies' classical theory by having a low relative energy, despite having $\varphi_i \cong -120°$ (better described as an eclipsing conformation, where the acetyl $C{=}O_{[i-1]}$ and the Cα hydrogen (C(α)-H) are the atoms eclipsed). Due to the trigonal planar structure of the acetyl C ($C{=}O_{[i-1]}$), the C_β side chain and $C{=}O_{[i]}$ and substituents do not eclipse the methyl carbon of the Ac group. Despite the 'energetic debit' due to the structural arrangement, the allowed intramolecular interactions stabilize the structure to the extent that it is at a genuine minimum, with a low relative energy.

The δ_D conformer does not show this φ_i structural probability due to the need for the acetyl $C{=}O_{[i-1]}$ and C_β−(Ar) atoms to eclipse. This conformation creates a very 'energetically costly' steric arrangement that could not be possibly recovered by any interaction facilitated by the 'classically forbidden' $\varphi = +120.0°$ backbone structure.

Accordingly, its relative energy is also much higher than both of the δ_L conformers, clearly indicating that there are very powerful stabilizing forces attributed to the δ_L structure, absent in the δ_D BB conformers.

3.3. Hydrogen Bonding and Other Intramolecular Interactions. The presence or absence of intramolecular H-bonding and weakly polar interaction may be qualitatively observed, for all optimized conformers, in Table 3. However, proximity of oppositely polarizable centers is not the sole determining factor of the presence, absence, or strength of H-bonding or weakly polar interaction. Geometric threshold separation may only be used as an indicator of a potential for interaction between polarizable centers. Sufficient MO overlap is required to support the claim of a stabilizing interaction; a reiteration of the observations made for the energetic results (Figures 5 and 6).

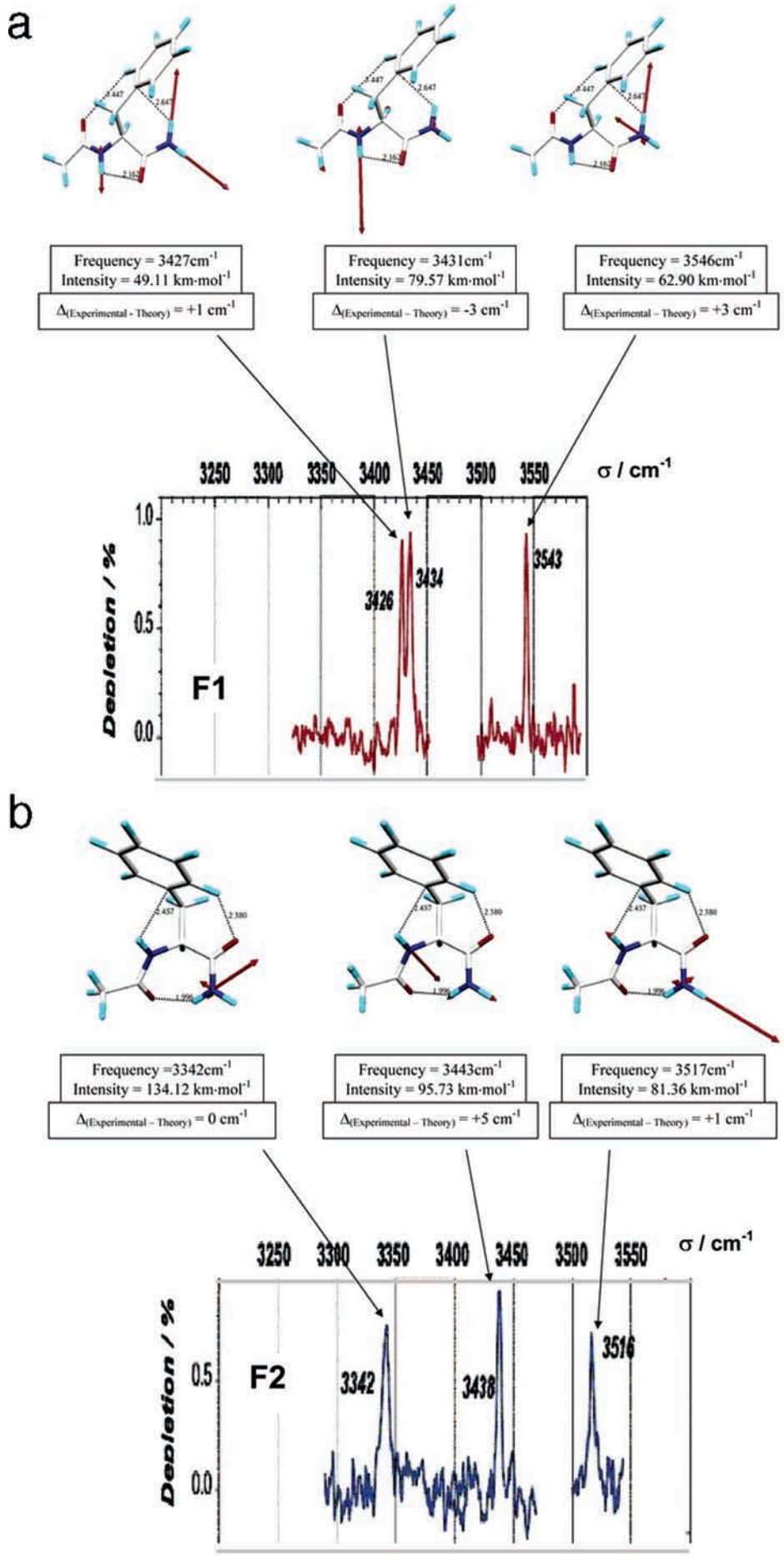
a
Frequency = 3427cm-1
Intensity = 49.11 km·mol-1
Δ(Experimental - Theory) = +1 cm-1
Frequency = 3431cm-1
Intensity = 79.57 km·mol-1
Δ(Experimental – Theory) = -3 cm-1
Frequency = 3546cm-1
Intensity = 62.90 km·mol-1
Δ(Experimental – Theory) = +3 cm-1
3250 3300 3350 3400 3450 3500 3550
σ / cm-1
1.0
0.5
0.0
Depletion / %
3426
3434
3543
F1
b
Frequency =3342cm-1
Intensity = 134.12 km·mol-1
Δ(Experimental – Theory) = 0 cm-1
Frequency = 3443cm-1
Intensity = 95.73 km·mol-1
Δ(Experimental – Theory) = +5 cm-1
Frequency = 3517cm-1
Intensity = 81.36 km·mol-1
Δ(Experimental – Theory) = +1 cm-1
3250 3300 3350 3400 3450 3500 3550
σ / cm-1
0.5
0.0
Depletion / %
F2
3342
3438
3516

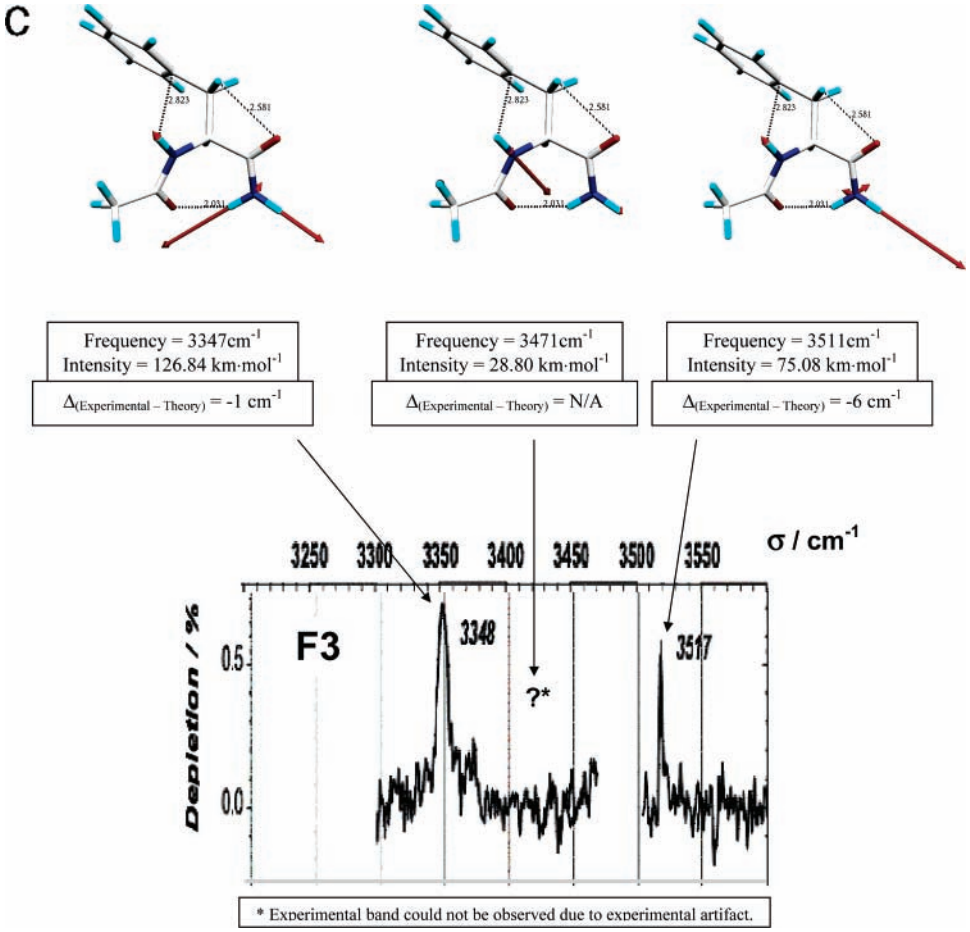

Figure 4. Comparison between experimental and computed IR spectra for the B3LYP/6-31+G(d) geometry optimized $\beta_L{}^{\alpha}$, $\gamma_L{}^{g+}$, and $\gamma_L{}^{g-}$ conformers of NAPA (parts a−c, respectively). Systematic conformational analysis resulted in accurate identification of these conformers as being candidate to most effectively reproduce experimentally determined normal modes of vibration. Dashed lines show selected intramolecular interaction distances (Å) within each conformer. Arrows show direction of force gradients associated with each normal mode of vibration. Computed frequencies have been corrected by a scaling factor of 0.960. Computed peak intensities and the difference between experimentally and theoretically determined vibrations are also shown.

Perusing Table 3, one finds that a trend is displayed, where interactions 'turn on and off' like switches, with classical structural ideals satisfied.

A number of the following 3.3 subsection results are presented and discussed in the context of AIM analyses (Section 3.5). The reader is encouraged to peruse Section 3.5 and to oscillate between all figures, tables, and discussions to have a complete set of results and observations.

3.3.1. Traditional Backbone−Backbone Interaction: C═O- - -H−N. The distances between the carbonyl oxygen (C═$O_{[i-1]}$, C═$O_{[i]}$) and amide H ($N_{[i]}$-H, $N_{[i+1]}$-H, $N_{[i+1]}$-H′) atoms are listed in Table 3. Both the β_L and γ_L BB conformations display distances common to this well-established BB−BB H-bond interaction (∼1.8−2.2 Å). More specifically C═$O_{[i]}$- - -H−$N_{[i]}$ and C═$O_{[i-1]}$- - -H−$N_{[i+1]}$ atoms are within these distances, for β_L and γ_L/γ_D, respectively; no other BB conformer is a candidate for these interaction types. These interactions can be observed in Figure 4a−c (dashed lines), Figure 5 (overlapping orbital 'lobes'), Figure 6 (density overlap in orbitals, indicated by ovals), and Figure 7a−c (indicated by arrows).

3.3.2. Aromatic-Amide Side Chain−Backbone Interaction: Ar- - -H−N. The interaction has previously been characterized as involving the C_γ atoms of the Phe side chain aromatic ring.[18] The distances between the aromatic C_γ and the three amide H ($N_{[i]}$-H, $N_{[i+1]}$-H, $N_{[i+1]}$-H′) atoms are listed for each level of theory, in columns 4, 5, and 6 in Table 3, defined as ($Ar_{[i]}$)-C_γ- - -H−$N_{[i+1]}$. These interactions can be observed in Figure 6 (density overlap in orbitals, indicated by ovals) and Figures 8 and 9 (indicated in the legends).

The $\beta_L{}^{a}$, $\gamma_L{}^{g+}$, $\gamma_L{}^{g-}$, $\delta_L{}^{g+}$, $\delta_D{}^{g+}$, and $\epsilon_D{}^{a}$ conformers all show a potential for this interaction; the first three also having the three lowest corrected-ZPE-scaled relative energies. A distance <3.0 Å was used as a 'scoring' criterion. Only the β_L conformer has AIM confirmed data for the existence of the interaction.

3.3.3. Alternate Backbone−Backbone Interaction: N- - -H−N. The distances between the amidic nitrogen ($N_{[i]}$, $N_{[i+1]}$) and amide hydrogen ($N_{[i]}$-H, $N_{[i+1]}$-H, $N_{[i+1]}$-H′) atoms are listed for each level of theory, in columns 7, 8, and 9 in Table 3. The amide- - -amidic-hydrogen interaction appears to be strongly stabilizing and directly responsible for the observed energetic trends of the δ_L conformers and their resultant low relative energy. The visualization of the δ_L structures, Figure 3b, shows the slight pyramidalization of the amidic $N_{[i]}$. Once again, satisfaction of geometric threshold separation may not be used as a sole determining factor for the presence of a true $N_{[i]}$- - -H−$N_{[i+1]}$ electrostatic interaction. An affirmation of an exchange of electronic probability density must be accurately identified and characterized.

The α_L, α_D, and ϵ_L conformers also show similar small geometric threshold separation (Table 3, columns 7, 8, and 9), making them a candidate for possible $N_{[i]}$- - -H−$N_{[i+1]}$ interaction. The AIM analysis was not extended to the δ_L, δ_D, α_L, α_D, and ϵ_L BB conformers; the ideal is a complete analysis of all stable conformers, including AIM analysis.

TABLE 1: Selected Backbone and Side Chain Dihedral Angles (Degrees) for N-Ac-Phe-NH_2 Geometry Optimized at the B3LYP/6-31G+(d) and BLYP/6-311G(df,p) Levels of Theory[a]

			ω_{i-1}		ø$_i$		χ_i^1		χ_i^2		ψ_i		ω_i	
BB	χ^1	χ^2	B3LYP/6-31+G (d)	BLYP/6-311G (df,p)	B3LYP/6-31+G (d)	BLYP/6-311G (df,p)	B3LYP/6-31+G (d)	BLYP/6-311G (df,p)	B3LYP/6-31+G (d)	BLYP/6-311G (df,p)	B3LYP/6-31+G (d)	BLYP/6-311G (df,p)	B3LYP/6-31+G (d)	BLYP/6-311G (df,p)
β	+	+	176.73	175.94	−156.17	−155.95	58.81	60.28	89.59	89.871	167.47	167.82	−175.31	−178.80
β	a	+	177.57	175.40	−158.32	−157.13	194.26	−159.15	67.55	71.25	162.34	166.44	172.44	174.37
β	-	+	N/F[b]	174.28	N/F[b]	−118.77	N/F[b]	−61.03	N/F[b]	94.80	N/F[b]	145.72	N/F[b]	179.60
	mean		−179.71	177.15	175.21	−157.25	−143.95	126.54	−173.30	78.57	85.31	164.91	159.99	178.57
	STDEV		5.46	0.59	0.85	1.52	21.81	95.78	119.97	15.58	12.42	3.63	12.38	8.66
γ_L	+	+	−175.49	−175.20	−81.88	−81.71	−316.29	−317.91	78.54	79.12	54.86	59.21	175.62	179.05
γ_L	a	+	179.74	−179.12	−82.62	−82.14	−164.96	−162.04	87.03	91.49	82.09	78.42	−170.76	−172.08
γ_L	-	+	−173.13	−173.85	−84.17	−83.17	−55.80	−53.38	114.72	112.04	73.44	73.21	−172.97	−173.66
	mean		−176.29	−176.29	−176.06	−82.89	−82.34	−179.02	−177.78	93.43	94.21	70.13	70.28	−56.04
	STDEV		3.63	3.63	2.74	1.17	0.75	130.81	132.96	18.92	16.63	13.91	9.94	200.62
γ_D	+	+	172.95	171.32	55.99	53.09	67.88	68.67	80.97	83.37	−25.36	−27.78	−174.57	−175.27
γ_D	a	+	176.73	176.98	73.48	72.34	−168.77	−170.18	82.50	84.59	−67.22	−66.50	173.68	175.16
γ_D	-	+	173.15	174.07	73.82	72.43	−58.95	−59.19	103.65	101.77	−52.42	−54.85	−177.98	−178.61
	mean		174.28	174.28	174.12	67.76	65.95	−173.28	−173.57	89.04	89.91	−48.33	−49.71	−179.62
	STDEV		2.13	2.13	2.83	10.20	11.14	116.65	116.11	12.68	10.29	21.23	19.86	6.04
α_L	+	+	−169.64	−171.66	−119.01	−121.85	53.87	54.02	81.47	83.66	15.83	18.81	171.84	174.52
α_L	-	+	−166.99	−168.53	−107.53	−114.15	−60.86	297.05	112.54	104.80	5.01	12.99	172.38	172.82
	mean		−168.32	−168.32	−170.10	−113.27	−118.00	−3.50	175.53	97.01	94.23	10.42	15.90	172.11
	STDEV		1.87	1.87	2.21	8.12	5.44	81.13	171.84	21.97	14.95	7.65	4.12	0.38
α_D	+	+	171.61	170.93	−163.73	−168.39	59.91	57.01	96.48	92.56	−38.57	−36.97	−170.78	−171.52
α_D	a	+	175.23	175.57	−154.28	−153.58	−174.47	−173.44	75.13	77.54	−59.87	−63.12	−172.65	−174.49
	mean		173.42	173.42	173.25	−159.01	−160.99	122.72	121.79	85.81	85.05	−49.22	−50.04	−171.72
	STDEV		2.56	2.56	3.28	6.68	10.47	88.83	91.60	15.10	10.62	15.06	18.49	1.32
α_L	a	+	−169.71	N/F[b]	−86.13	N/F[b]	−170.33	N/F[b]	75.43	N/F[b]	−24.12	N/F[b]	171.67	N/F[b]
α_D	+	+	165.23	167.71	49.50	47.39	51.49	48.70	81.70	80.74	41.01	45.16	−172.58	−172.47
α_D	a	+	170.90	170.87	68.18	63.77	−131.20	−137.08	102.38	100.44	31.85	38.62	−173.38	−174.09
α_D	-	+	N/F[b]	167.87	N/F[b]	69.04	N/F[b]	−62.32	N/F[b]	101.32	N/F[b]	27.45	N/F[b]	−174.89
	mean		170.37	168.07	168.82	58.84	60.07	140.15	69.77	92.04	94.17	36.43	37.08	−172.98
	STDEV		4.89	4.01	1.78	13.21	11.29	125.38	143.78	14.62	11.63	6.48	8.95	0.57
ϵ_D	a	+	−163.67	−162.52	64.85	65.95	−157.24	−158.10	60.64	61.13	−168.84	−167.54	−179.66	−176.93

[a] The means and standard deviations for each backbone conformer are also shown where applicable. Note: means and standard deviations are not computed or shown for χ_i^1 due to the organization of the data by backbone conformation. [b] N/F indicates conformer not found at the level of theory.

TABLE 2: Total Energy (Hartrees), Relative Energy (kcal*mol^{-1}), and Corrected ZPE (Hartree)-Adjusted Rel. E. (kcal*mol^{-1}) for Stable Backbone and Side Chain Conformations of N-Ac-Phe-NH_2 at the B3LYP/6-31G+(d) and BLYP/6-311G(df,p) Levels of Theory

			total energy (Hartrees)		relative energy (kcal*mol^{-1})		zero-point energy ZPE (Hartree/particle)		scaled by 0.967 ZPE corrected SCF (Hartrees)		scaled ZPE-corrected relative energy (kcal*mol^{-1})	
BB	χ1	χ2	B3LYP/6-31+G (d)	BLYP/6-311G (df,p)	B3LYP/6-31+G (d)	BLYP/6-311G (df,p)	B3LYP/6-31+G (d)	BLYP/6-311G (df,p)	B3LYP/6-31+G (d)	BLYP/6-311G (df,p)	B3LYP/6-31+G (d)	BLYP/6-311G (df,p)
β	+	+	−687.62181	−687.54838	2.32	2.60	0.239391	0.231188	−687.39032	−687.324821	2.16	1.95
β	a	+	−687.62550	−687.55163	0.00	0.56	0.239646	0.231567	−687.39376	−687.327709	0.00	0.14
β	-	+	N/F[a]	−687.54756	N/F[a]	3.12	N/F[a]	0.231040	N/F[a]	−687.324144	N/F[a]	2.37
γ_L	+	+	−687.62523	−687.55253	0.17	0.00	0.240465	0.232271	−687.3927	−687.327925	0.67	0.00
γ_L	a	+	−687.62470	−687.55174	0.50	0.50	0.240053	0.231899	−687.39257	−687.327494	0.75	0.27
γ_L	-	+	−687.62494	−687.55166	0.35	0.55	0.240002	0.231795	−687.39286	−687.327512	0.57	0.26
γ_D	+	+	−687.61407	−687.54125	7.18	7.08	0.240479	0.231843	−687.38152	−687.317053	7.68	6.82
γ_D	a	+	−687.61959	−687.54648	3.71	3.80	0.240161	0.231927	−687.38735	−687.322204	4.02	3.59
γ_D	-	+	−687.62281	−687.54921	1.69	2.09	0.240446	0.232184	−687.3903	−687.324683	2.17	2.03
δ_L	+	+	−687.62278	−687.54939	1.71	1.97	0.240102	0.231643	−687.3906	−687.325389	1.99	1.59
δ_L	-	+	−687.62085	−687.54702	2.92	3.46	0.239457	0.231032	−687.38929	−687.323614	2.81	2.70
δ_D	+	+	−687.61598	−687.54196	5.97	6.63	0.239767	0.231727	−687.38413	−687.317878	6.04	6.30
δ_D	a	+	−687.61382	−687.54020	7.33	7.74	0.239241	0.230933	−687.38247	−687.316885	7.09	6.93
α_L	a	+	−687.61489	N/F[a]	6.66	N/F[a]	0.239242	N/F[a]	−687.38354	N/F[a]	6.41	N/F[a]
α_D	+	+	−687.61104	−687.53854	9.08	8.78	0.239876	0.231436	−687.37908	−687.314741	9.21	8.27
α_D	a	+	−687.61391	−687.54124	7.28	7.08	0.239768	0.231248	−687.38205	−687.317626	7.35	6.46
α_D	-	+	N/F[a]	−687.54441	N/F[a]	5.09	N/F[a]	0.231271	N/F[a]	−687.320774	N/F[a]	4.49
ϵ_D	a	+	−687.61468	−687.54074	6.79	7.40	0.239557	0.231304	−687.38303	−687.317068	6.74	6.81

[a] N/F indicates conformer not found at the level of theory.

3.3.4. Alternate Side Chain−Backbone Interactions: C═O- - -H−R. The distances between the carbonyl oxygen (C═O$_{[i-1]}$, C═O$_{[i]}$) and phenyl H (*H*−C$_\delta$-*(Ar)*) atoms are not tabulated nor listed in this work. The data were not collected nor presented, as the interaction was not predicted as being significant in the NAPA system. However, the potential for the C═O$_{[i-1]}$- - -H−

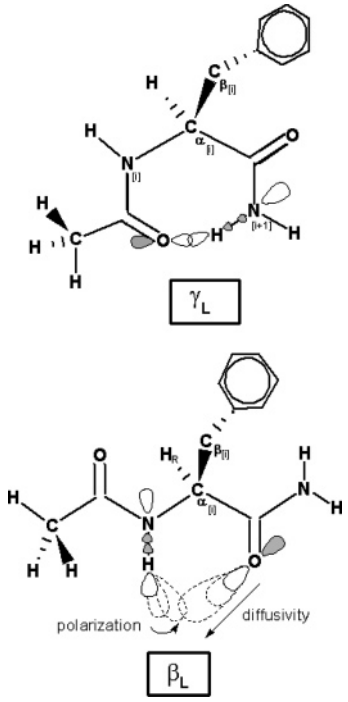

Figure 5. Schematic representation of the expected energetic stabilization attributed to the basis set employed in the geometry optimization of the γ_L (*top*) and β_L backbone conformers (*bottom*) of NAPA. Although qualitative, the diagram shows how employing basis sets including polarization and diffuse functions can more significantly stabilize one conformer relative to another. This is due to atomic and molecular orbital alignments and symmetries of the *p*-orbitals of O and the σ^* orbitals of the amidic H, influenced by their geometries. In the γ_L conformer, there may be a higher degree of orbital (MO) overlap inherent to the structure, relative to the β_L conformer. Therefore, one may predict from simple diagrams and basic theoretical principles that the γ_L conformer would be more significantly stabilized than the β_L conformer, using less mathematically complete basis sets. More complete basis sets may therefore lower the energy of the β_L conformer more significantly than the γ_L conformer.

CHART 3

	Experimental		B3LYP/6-31+G(d)		BLYP/6-311G(df,p)		
A	1694	1725	1695	1725	1661	1694	$\beta_L{}^a$
B	1682	1718	1685	1725	1648	1694	$\gamma_L{}^{g+}$
C	1680	1719	1687	1736	1650	1706	$\gamma_L{}^{g-}$
			→	1722/1726	→	1693/1694	$\delta_L{}^{g+}$

C_δ-($Ar_{[i]}$) and (C═$O_{[i]}$- - -H−C_δ-($Ar_{[i]}$) interactions to be present emerged from AIM analyses of the $\beta_L{}^a$ and $\gamma_L{}^{g+}$ conformers. These interactions can be observed in Figure 4a−c (dashed lines), Figure 6 (density overlap in orbitals, indicated by ovals), and Figure 7a,b (indicated by arrows). Further investigation is required to more accurately characterize the existence and nature of these interactions.

3.4. Experimental and Theoretical IR Frequencies. The computed frequencies of selected normal modes of vibration are listed in Table 4; N-$H_{[i+1]}$-symmetric, N−$H_{[i]}$, N−$H_{[i+1]}$-anti-symmetric stretches are found in columns 1, 3, and 5, respectively. The C═$O_{[i-1]}$, C═$O_{[i]}$ stretches and N−$H_{[i]}$, N−$H_{[i+1]}$, N−$H'_{[i+1]}$ are found in Table 5 and Supporting Information tables, respectively. Corresponding intensities (km*mol^{-1}) are found to the right of each frequencies' columnated results.

The experimentally determined N−H stretch spectral region (3200−3600 cm^{-1}) are displayed in Figure 4−c. Carbonyl stretches are reported in Chart 3. Qualitatively, one may observe that the theoretically determined IR intensities match well with the visual size of the absorption peaks. More in-depth description, presentation, and analyses of these experimentally determined results can be found in the accompanying work.[72]

Established literature recommends that frequency scaling-factors of 0.96 should be applied to the B/6+ geometry optimized frequencies.[44] The 0.96-fraction scales each of the 9 N−H stretch frequencies, of the $\beta_L{}^a$, $\gamma_L{}^{g+}$, and $\gamma_L{}^{g-}$ conformers to within 0−6 cm^{-1}.

The 0.96-fraction does not provide numerical agreement between the experimental and for the theoretically determined B/6+ frequencies. Rather, if one applies a 0.98 scaling-factor, the C═$O_{[i-1]}$, C═$O_{[i]}$ stretches show acceptable numerical agreement with the experimental ones. Using the 0.98 scaling-factor in conjunction with the frequencies in Table 5, one finds that the experimentally C═O-stretch-determined conformers A, B, and C agree relatively well with the $\beta_L{}^a$, $\gamma_L{}^{g+}$, and $\gamma_L{}^{g-}$ structural conformers, respectively. Chart 3 shows the experimental and 0.98-scaled theoretical C═$O_{[i-1]}$ and C═$O_{[i]}$ frequencies (cm^1) for the B/6+ level, the lower and higher values, respectively. Unscaled L/61fp results are also shown.

The C═$O_{[i-1]}$ and C═$O_{[i]}$ frequencies for the $\delta_L{}^{g+}$ conformer are also shown scaled by a factor of 0.98 for the B/6+ level and unscaled for L/61fp results. The C═$O_{[i-1]}$ and C═$O_{[i]}$ frequencies are shifted to approximately 1722 cm^{-1} and 1726 cm^{-1}, respectively (Chart 3), matching well with the experimentally determined C═$O_{[i]}$ stretch. No other conformer shows this C═O near 'stretch degeneracy' (Table 5). Additionally, the conformer shows degeneracy in its H−$N_{[i]}$ and H−$N_{[i+1]}{}^{symmetric}$ stretches.

The $\delta_L{}^{g+}$ conformer requires a more thorough theoretical characterization, as mentioned in the structural analysis (section *3.1*), if only to uncover the basis of the near-degeneracy of the two C═O and H−N stretches.

3.5. Electron Populations and Orbital Overlap. Surface plots of the electron density distribution are shown in Figure 6. Although the diagrams only provide a qualitative illustration of the density distribution of each static geometric 'pose', they provide a feeling for the specificity and limited nature of certain intramolecular interactions. The results also show that the level of theory, and more particularly the influence of the basis set applied, plays a dominant role in determining the degree of density overlap observed between polarized centers. Once again a lengthy text description is much inferior to a quick observation of the difference between the structures on the left and right portions of the upper part of Figure 6.

The structures in Figure 6 have been aligned in viewing space to show the interactions, where they exist. The AIM predicted C═$O_{[i-1]}$- - -H−C_δ-($Ar_{[i]}$) interaction in the $\beta_L{}^a$ conformer was not confirmed by electron population analysis as no overlap in density was observed. Inversely, the $\gamma_L{}^{g+}$ and $\gamma_L{}^{g-}$ conformers show density overlap consistent with the (Ar)-C_γ- - -H−$N_{[i]}$ interaction, where the AIM analysis does not show the existence of this interaction.

3.6. Atoms-In-Molecules (AIM) Analysis. The bond paths emerging from Atoms-In-Molecules analysis of the input wave functions are structurally depicted in Figure 7a−c. These diagrams show the Bond Critical Points (BCPs) as (red) dots, found on the line joining two atoms. Ring Critical Points (RCPs) are also shown as (yellow) dots, found at the center of intramolecular rings formed either via covalent or ionic bonding.

Figure 7a shows the $\beta_L{}^a$ conformer as having 5-, 6-, and 8-membered rings formed by the following intramolecular

TABLE 3: Interatomic Distances for Selected Intramolecular Interactions (Å) for Geometry Optimized Conformers of N-Ac-Phe-NH_2 at the B3LYP/6-31G+(d) and BLYP/6-311G(df,p) Levels of Theory

			$C{=}O_{[i-1]}\text{- - -}H{-}N_{[i+1]}$ (Å)		$C{=}O_{[i-1]}\text{- - -}H'\text{-}N_{[i+1]}$ (Å)		$C{=}O_{[i]}\text{- - -}H{-}N_{[i]}$ (Å)		$Ar{-}C_{\gamma[i]}\text{- - -}H{-}N_{[i]}$ (Å)		$Ar{-}C_{\gamma[i]}\text{- - -}H{-}N_{[i+1]}$ (Å)	
BB	χ^1	χ^2	B3LYP/ 6-31+G (d)	BLYP/ 6-311G (df,p)	B3LYP/ 6-31+G (d)	BLYP/ 6-311G (df,p)	B3LYP/ 6-31+G (d)	BLYP/ 6-311G (df,p)	B3LYP/ 6-31+G (d)	BLYP/ 6-311G (df,p)	B3LYP/ 6-31+G (d)	BLYP/ 6-311G (df,p)
β	+	+	6.05	6.10	5.04	5.08	2.19	2.18	3.36	3.40	4.07	4.01
β	a	+	6.08	6.11	5.08	5.11	2.16	2.15	4.51	4.55	2.65	2.66
β	-	+	N/F[a]	5.48	N/F[a]	4.40	N/F[a]	2.42	N/F[a]	3.66	N/F[a]	4.56
γ_L	+	+	3.75	3.74	2.00	1.99	3.88	3.86	2.46	2.46	4.96	5.00
γ_L	a	+	3.76	3.74	2.16	2.10	3.44	3.53	4.11	4.12	4.59	4.65
γ_L	-	+	3.71	3.72	2.03	2.02	3.72	3.74	2.82	2.82	5.05	5.07
γ_D	+	+	3.58	3.58	1.83	1.80	4.25	4.29	3.96	3.95	3.52	3.49
γ_D	a	+	3.66	3.67	1.97	1.96	3.77	3.82	4.49	4.51	3.94	3.94
γ_D	-	+	3.69	3.69	1.94	1.93	3.99	4.00	3.44	3.46	4.43	4.42
δ_L	+	+	4.94	5.04	3.53	3.60	4.04	4.03	2.65	2.70	4.39	4.44
δ_L	-	+	4.70	4.86	3.39	3.46	4.18	4.11	3.03	3.24	5.01	5.09
δ_D	+	+	5.96	5.99	4.81	4.77	3.59	3.60	3.66	3.72	2.76	2.87
δ_D	a	+	6.00	6.05	5.01	5.05	3.45	3.46	4.53	4.54	3.65	3.65
α_L	a	+	4.40	N/F[a]	3.41	N/F[a]	4.35	N/F[a]	4.00	N/F[a]	4.70	N/F[a]
α_D	+	+	3.51	3.54	2.67	2.84	4.46	4.48	3.55	3.57	4.76	4.85
α_D	a	+	3.94	3.92	3.10	3.23	4.42	4.46	4.05	4.11	5.15	5.12
α_D	-	+	N/F[a]	3.97	N/F[a]	3.08	N/F[a]	4.46	N/F[a]	3.25	N/F[a]	5.11
ϵ_D	a	+	4.76	4.82	4.46	4.53	2.76	2.86	4.55	4.57	2.40	2.40

			$Ar{-}C_{\gamma[i]}\text{- - -}H'\text{-}N_{[i+1]}$ (Å)		$N_{[i]}\text{- - -}H{-}N_{[i+1]}$ (Å)		$N_{[i]}\text{- - -}H'\text{-}N_{[i+1]}$ (Å)		$N_{[i+1]}\text{- - -}H{-}N_{[i]}$ (Å)	
BB	χ^1	χ^2	B3LYP/ 6-31+G(d)	BLYP/ 6-311G(df,p)	B3LYP/ 6-31+G(d)	BLYP/ 6-311G(df,p)	B3LYP/ 6-31+G(d)	BLYP/ 6-311G(df,p)	B3LYP/ BLYP/	BLYP/ 6-311G(df,p)
β	+	+	4.59	4.56	3.98	4.01	4.43	4.46	3.79	3.79
β	a	+	4.02	4.12	3.99	4.01	4.43	4.46	3.76	3.77
β	-	+	N/F[a]	5.57	N/F[a]	3.88	N/F[a]	4.43	N/F[a]	3.89
γ_L	+	+	5.33	5.39	2.74	2.77	3.90	3.93	3.68	3.74
γ_L	a	+	4.99	5.08	2.96	2.92	3.94	3.95	3.83	3.83
γ_L	-	+	5.89	5.92	2.86	2.86	3.93	3.95	3.89	3.90
γ_D	+	+	4.44	4.41	2.71	2.72	3.98	4.03	3.85	3.92
γ_D	a	+	4.52	4.52	2.84	2.85	3.95	3.99	3.88	3.91
γ_D	-	+	5.54	5.56	2.77	2.79	3.96	3.99	3.83	3.87
δ_L	+	+	4.91	4.95	2.35	2.36	3.76	3.78	3.11	3.11
δ_L	-	+	5.83	5.90	2.34	2.36	3.76	3.78	3.22	3.16
δ_D	+	+	4.03	4.12	2.69	2.65	3.79	3.80	2.42	2.44
δ_D	a	+	4.43	4.46	2.94	2.98	3.88	3.91	2.59	2.64
α_L	a	+	4.92	N/F[a]	2.36	N/F[a]	3.75	N/F[a]	3.29	N/F[a]
α_D	+	+	5.21	5.29	2.50	2.52	3.83	3.84	3.70	3.71
α_D	a	+	5.51	5.48	2.39	2.43	3.76	3.78	3.46	3.51
α_D	-	+	N/F[a]	5.91	N/F[a]	2.39	N/F[a]	3.79	N/F[a]	3.52
ϵ_D	a	+	4.08	4.10	4.05	4.08	4.48	4.52	4.12	4.19

[a] N/F indicates conformer not found at the level of theory.

interactions: $C{=}O_{[i]}\text{- - -}H{-}N_{[i]}$, $(Ar_{[i]})\text{-}C_\gamma\text{- - -}H{-}N_{[i+1]}$, $C{=}O_{[i-1]}\text{- - -}H{-}C_\delta\text{-}(Ar_{[i]})$, respectively.

Figure 7b shows the $\gamma_L{}^{g+}$ conformer as having two 7-membered rings formed by the following intramolecular interactions: $C{=}O_{[i-1]}\text{- - -}H{-}N_{[i+1]}$ and $C{=}O_{[i]}\text{- - -}H{-}C_\delta\text{-}(Ar_{[i]})$, respectively.

Figure 7c shows the $\beta_L{}^a$ conformer as having a 7-membered ring formed by the $C{=}O_{[i]}\text{- - -}H{-}N_{[i]}$ intramolecular interaction.

3.7. Comparison of Structure and Energy of Ac-Gly-NH_2, Ac-Ala-NH_2, and Ac-Phe-NH_2. The nature and magnitude of the structural and energetic trends for Ac-Gly-NH_2, Ac-Ala-NH_2, and Ac-Phe-NH_2, geometry optimized at the B3LYP/6-31+G(d) and MP2/6+ levels of theory, may be observed in Table 6. Energetic trends are in qualitative agreement with one another in regards to the ordering by relative energy. Quantitatively, the largest difference is found between the B/6+ and M/6+ geometry optimized Gly β_L conformer (ΔEnergy $\cong$ 1.31 kcal*mol^{-1}). MP2/6+ frequency calculations were not completed for the Phe systems; therefore, frequency and ZPE values were not obtained for the Phe systems, thus no ZPE values are presented.

3.7.1. Structural Trends of Ac-Gly-NH_2, Ac-Ala-NH_2, and Ac-Phe-NH_2. Backbone dihedral angles for Ala and Phe have more similarity than those of Gly. This may be attributed to the lack of a heavy atom in the β-position of the side chain of Gly. The ω_{i-1} and ω_i dihedral angles show enantiospecific trends in their deviation from planarity of the peptide bond.

3.7.2. Energetic Trends of Ac-Gly-NH_2, Ac-Ala-NH_2, and Ac-Phe-NH_2. The Gly model shows the γ_L conformer to be 0.92 and 2.23 kcal*mol^{-1} lower in energy than the β_L conformer, at the B/6+ and M/6+ levels of theory, respectively. The Ala model shows the γ_L conformer to be 1.19 and 1.72 kcal*mol^{-1} lower in energy than the β_L conformer, at the B/6+ and M/6+ levels of theory, respectively. The lack of an aromatic side chain in Gly and Ala may be responsible for this difference in energetic ordering. Further investigation is necessary to provide an accurate energetic partitioning of all.

4. Conclusion

An accurate synergy has emerged between theory and experiment, owing its accuracy to the exhaustive MDCA-directed

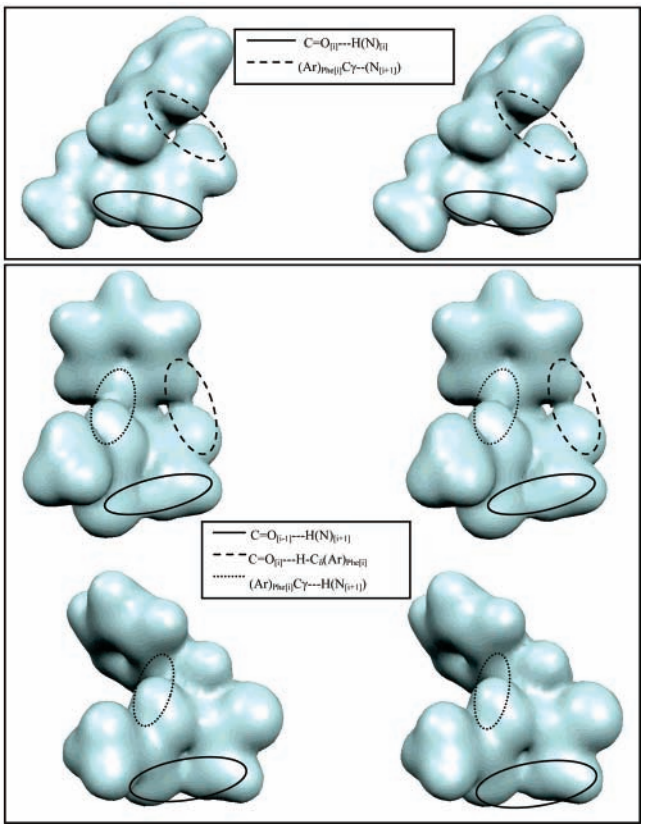

Figure 6. Molecular orbital (MO) population surfaces constructed from the electron density matrices emerging from the population analyses of the B3LYP/6-31G(d,p) (*left side*) and B3LYP/6-31+G(d) (*right side*) geometry optimized conformers of NAPA. Surfaces were constructed using a cutoff value of 0.0098. The $\beta_L{}^a$ conformer (*top*) shows orbital overlap and density for the C═$O_{[i]}$- - -H(N)$_{[i]}$ interaction; the (Ar)-Phe$_{[i]}C_\gamma$- - -H($N_{[i+1]}$) interaction shows overlap only in the population analysis of the 6-31G(d,p) optimized geometry (*top left*) but not in the 6-31+G(d) optimized geometry (*top right*). The $\gamma_L{}^{g+}$ conformer (*middle*) shows orbital overlap and density between the following pairs of nuclei: C═$O_{[i-1]}$- - -H(N)$_{[i+1]}$, C═$O_{[i]}$- - -H−C_δ(Ar)Phe$_{[i]}$.. The γL^{g-} conformer (*bottom*) shows orbital overlap and density between the following pairs of atoms: C═$O_{[i-1]}$- - -H(N)$_{[i+1]}$, C═$O_{[i]}$- - -HR−C_β. All interactions are identified by an elipse with their corresponding labels.

conformational searches carried out combined with exhaustive and continual refinements of experimental techniques and procedures. Theoretical precision was achieved through the use of an established, modular, explicit, and numeric methodology[3,4] and shows all expected trends for transferability to other model peptide systems.

Most promising for the numerical technique is its ability to predict, locate, and help to optimize transition state structures, between stable backbone and side chain conformers. Interconformational transition states are currently under investigation and are expected to help in the characterization of the kinetics that these systems undergo at higher temperatures.

The conformational searches for stable minima were successful at both characterizing the conformational probability of the NAPA model as well as providing insight into the electrostatic origins of stability, specifically, characterization of the aromatic-amide (Ar- - -HN) interaction as involving the C_γ of the phenylalanyl-side chain aromatic ring, in agreement with the literature[18] and experimental values for the H−N stretch. This is in addition to the novel characterization of the (Ar$_{[i]}$)-C_δ-H- - -O═$C_{[i+1]}$ and $N_{[i]}$- - -$HN_{[i+1]}$ interactions. The combined use of conformational, orbital population, and AIM

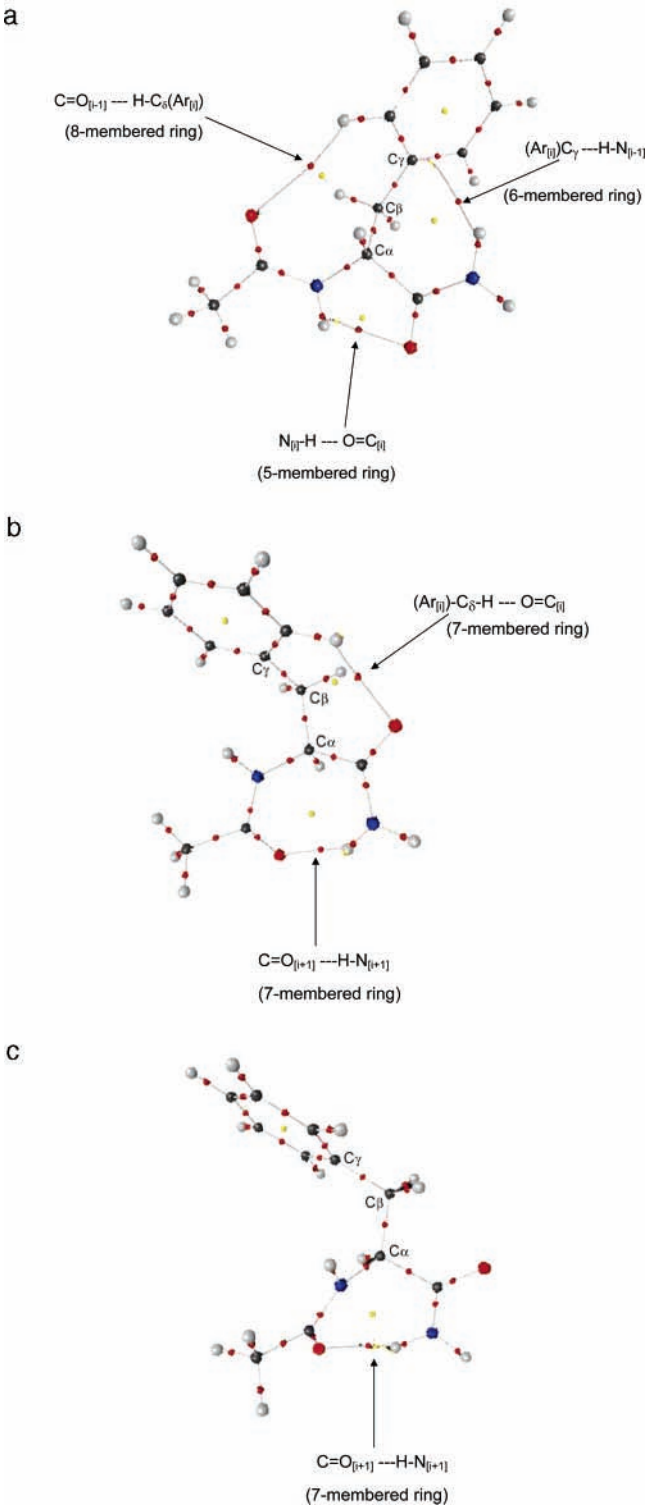

Figure 7. Atoms-In-Molecules (AIM) analysis of the bonding in NAPA emerging from the wave function generated from the geometry optimized $\beta_L{}^\alpha$, $\gamma_L{}^{g+}$, and $\gamma_L{}^{g+}$ conformers (parts a−c, respectively), at the B3LYP/6-31G(d,p) level of theory. Bond-Critical-Points (BCP), Ring-Critical-Points (RCP), and Cage-Critical-Points (CCP) are shown, with $\nabla\rho\bar{e} = 0$ (No flux in electron density) between two nuclei defining a bond. BCPs are observed between the following sets of atoms for each conformer, providing further evidence for the following intramolecular interactions: $\beta_L{}^a \rightarrow$ C═$O_{[i]}$- - -H(N)$_{[i]}$, C═$O_{[i-1]}$- - -H−C_δ-(Ar)$_{Phe[i]}$, (Ar)$_{Phe[i]}C_\gamma$- - -H($N_{[i+1]}$) $\gamma_L{}^+ \rightarrow$ C═$O_{[i]}$- - -H(N)$_{[i]}$, C═$O_{[i-1]}$- - -H−C_δ(Ar)$_{Phe[i]}$ $\gamma_L{}^- \rightarrow$ C═$O_{[i]}$- - -H(N)$_{[i]}$.

analyses allowed for efficient—yet incomplete—characterization of the interactions.

TABLE 4: Frequency and Corresponding Peak Intensities for $N_{[i]}$-H and $N_{[i+1]}$-H Stretches for Stable Backbone and Side Chain Conformations of N-Ac-Phe-NH_2 Geometry Optimized at the B3LYP/6-31G+(d) and BLYP/6-311G(df,p) Levels of Theory

			$N_{[i+1]}$-H symmetric stretch frequency (cm^{-1})		corresponding IR intensity (km/mol)		$N_{[i]}$-H symmetric stretch frequency (cm^{-1})		corresponding IR intensity (km/mol)		$N_{[i+1]}$-H antisymmetric stretch frequency (cm^{-1})		corresponding IR intensity (km/mol)	
BB	$\chi 1$	$\chi 2$	B3LYP/ 6-31+G (d)	BLYP/ 6-311G (df,p)	B3LYP/ 6-31+G (d)	BLYP/ 6-311G (df,p)	B3LYP/ 6-31+G (d)	BLYP/ 6-311G (df,p)	B3LYP/ 6-31+G (d)	BLYP/ 6-311G (df,p)	B3LYP/ 6-31+G (d)	BLYP/ 6-311G (df,p)	B3LYP/ 6-31+G (d)	BLYP/ 6-311G (df,p)
β	+	+	3577.9270	3469.1707	54.1110	70.1378	3582.7820	3486.4606	67.9710	28.6121	3702.1570	3614.1901	38.3670	26.5730
β	a	+	3570.5100	3458.1358	49.1070	82.1055	3574.8430	3471.6650	79.5710	29.5084	3694.3950	3598.0702	62.9030	51.0813
β	-	+	N/F[a]	3478.3780	N/F[a]	23.2372	N/F[a]	3489.1229	N/F[a]	34.2192	N/F[a]	3607.7910	N/F[a]	21.8266
γ_L	+	+	3481.0720	3353.6832	134.1160	135.9209	3586.6540	3486.8953	95.7330	83.9932	3663.3300	3560.5681	81.3590	53.6333
γ_L	a	+	3513.3110	3388.5335	84.1020	90.7427	3609.4880	3511.1472	24.6110	16.7312	3658.6850	3554.2049	65.5130	47.2269
γ_L	-	+	3486.3340	3364.3381	126.8380	122.6115	3615.2220	3517.0455	28.7990	22.1489	3657.1000	3552.9638	75.0850	47.9273
γ_D	+	+	3417.5970	3264.7907	266.5220	307.4132	3616.6430	3506.8267	23.1400	14.5113	3639.2550	3538.9353	83.4360	52.8538
γ_D	a	+	3477.9060	3352.3669	158.0650	158.2938	3623.6600	3525.6895	27.0860	18.6639	3653.4230	3550.9215	77.2090	51.3970
γ_D	-	+	3475.8900	3346.8369	165.8500	165.4869	3629.3260	3529.8588	26.1650	18.4935	3663.5760	3558.0135	92.9980	58.7556
δ_L	+	+	3583.6080	3488.3733	41.6690	18.7995	3587.2150	3489.4493	38.1900	30.5442	3715.2250	3619.8833	58.2830	42.3169
δ_L	-	+	3585.2910	3487.0192	31.1950	16.3998	3593.9990	3499.1132	16.7540	9.5762	3712.3050	3616.4718	61.3700	42.2104
δ_D	+	+	3538.4830	3444.7415	30.1070	15.3795	3610.1300	3506.5499	33.0880	23.4875	3652.0990	3561.9769	44.0810	27.5724
δ_D	a	+	3560.4220	3466.3187	26.6230	13.6282	3617.3670	3519.1395	31.0500	20.6570	3678.9560	3588.5221	31.1770	20.2206
α_L	a	+	3571.3510	N/F[a]	28.9140	N/F[a]	3594.4220	N/F[a]	18.5030	N/F[a]	3691.6420	N/F[a]	46.4330	N/F[a]
α_D	+	+	3569.6400	3474.7956	26.3530	14.7373	3603.7480	3503.4283	14.8290	9.0077	3684.6580	3591.0447	35.5590	24.2336
α_D	a	+	3578.8920	3480.8619	29.9250	15.6998	3609.0520	3502.3932	17.8760	8.9525	3700.0040	3603.4496	45.1670	31.2483
α_D	-	+	N/F[a]	3485.9118	N/F[a]	14.4586	N/F[a]	3505.2101	N/F[a]	10.3340	N/F[a]	3610.7527	N/F[a]	34.3217
ϵ_D	a	+	3568.4340	3461.9913	75.8570	62.8132	3601.2010	3500.3882	19.9700	11.6278	3694.3010	3591.6445	128.1230	93.0635

[a] N/F indicates conformer not found at the level of theory.

TABLE 5: Frequency and Corresponding Peak Intensities for $C{=}O_{[i-1]}$ and $C{=}O_{[i]}$ Stretches, for Stable Backbone and Side Chain Conformations of N-Ac-Phe-NH_2 Geometry Optimized at the B3LYP/6-31G+(d) and BLYP/6-311G(df,p) Levels of Theory

			$C{=}O_{[i-1]}$ stretch frequency (cm^{-1})		corresponding IR intensity (km/mol)		$C{=}O_{[i]}$ stretch frequency (cm^{-1})		corresponding IR intensity (km/mol)	
BB	χ^1	χ^2	B3LYP/ 6-31+G(d)	BLYP/ 6-311G(df,p)	B3LYP/ 6-31+G(d)	BLYP/ 6-311G(df,p)	B3LYP/ 6-31+G(d)	BLYP/ 6-311G(df,p)	B3LYP/ 6-31+G(d)	BLYP/ 6-311G(df,p)
β	+	+	1731.66302	1665.0533	359.9030	270.6661	1769.527	1700.2870	195.6570	142.4120
β	a	+	1729.5300	1660.699	357.5110	256.6636	1760.0930	1693.6116	267.7880	208.0635
β	-	+	N/F[a]	1683.7046	N/F[a]	302.0460	N/F[a]	1700.4956	N/F[a]	118.6508
γL	+	+	1719.0870	1647.7092	210.0160	139.3216	1759.9200	1694.0799	408.2510	325.1595
γL	a	+	1724.1610	1651.9727	183.3480	125.9077	1770.0250	1700.8955	378.7280	302.9082
γL	-	+	1721.1080	1649.8019	188.0930	130.8634	1769.9580	1706.4150	414.9870	310.5188
γ_D	+	+	1742.9140	1673.6443	112.1490	78.8194	1753.5560	1692.7594	425.8650	321.0451
γ_D	a	+	1727.0960	1653.4694	135.6340	94.4640	1767.7660	1708.0507	410.0870	297.5544
γ_D	-	+	1724.3460	1651.0624	128.3170	91.5684	1758.8310	1702.5270	459.9810	329.5387
δ_L	+	+	1757.6780	1692.6629	305.0980	218.2842	1761.9610	1694.2007	348.7500	279.2317
δ_L	-	+	1763.4590	1697.4515	267.3380	174.3204	1765.5880	1701.0380	343.3440	280.6550
δ_D	+	+	1750.3430	1680.6280	238.5280	131.8623	1783.3430	1715.5527	363.9710	249.3254
δ_D	a	+	1748.7270	1679.6394	229.9410	170.2479	1790.5300	1721.2942	298.6180	233.3680
α_L	a	+	1765.0800	N/F[a]	231.7410	N/F[a]	1783.3220	N/F[a]	336.9710	N/F[a]
α_D	+	+	1766.5990	1696.5259	210.45503	131.862	1774.4290	1706.2830	275.8570	249.3254
α_D	a	+	1761.331	1693.0211	193.8800	129.3567	1776.0030	1708.4913	336.1940	279.0296
α_D	-	+	N/F[a]	1692.0334	N/F[a]	146.4486	N/F[a]	1708.9333	N/F[a]	269.8098
ϵ_D	a	+	1756.8300	1693.2256	454.4770	282.1142	1768.8960	1706.8686	147.5480	173.484

[a] N/F indicates conformer not found at the level of theory.

The long-standing and ongoing debate about which method and basis set is best used (in order to achieve the minimal accuracy required to properly characterize the model peptide systems) has not been brought any closer to being satisfied. An excellent qualitative correlation with experimental results was achieved using the B3LYP method, employing the 6-31G(d), 6-31G(d,p), and 6-31+G(d) levels of theory, this is reflected at the BLYP/6-311G(df,p) level. Quantitative 'certainty' would require, by definition, an infinite basis set.

Future and continued work on the complete characterization of NAPA would benefit from an 'automated iterative process' of steps, until theoretical refinement suffers from a 'law of diminishing returns'; instead of where accuracy would not be sufficiently ameliorated to justify the computational resources expended. Clearly this is an 'era-dependent' factor, where computational resources are continually evolving, facilitating today that which was computationally unattainable yesterday.

A second 'offshoot' of this work may include the evaluation of conformer- and computational level-dependent force constants, associated with each degree of freedom. The level of theory generating results most accurately and precisely in agreement with experimental values may be used to reparametrize existing force-fields for peptide systems. Once the complete set of N- and C-protected amino acids have been so

TABLE 6: Selected Backbone Dihedral Angles (Degrees), Total Energy (Hartrees), and Relative Energy (kcal*mol^{-1}) for N-Ac-Gly-NH_2, N-Ac-Ala-NH_2, and N-Ac-Phe-NH_2, Geometry Optimized at the B3LYP/6-31G+(d) and MP2/6-31G+(d) Levels of Theory, Labeled B/6+ and M/6+, Respectively

	ω_{i-1}		φ_i		ψ_i		ω_i		total energy (Hartrees)		relative energy (kcal*mol^{-1})	
	B/6+	M/6+	B/6+	M/6+	B/6+	M/6+	B/6+	M/6+	B/6+	M/6+	B/6+	M/6+
						β						
Gly	180.00	180.00	180.00	180.00	180.00	180.00	180.00	180.00	−417.2489085	−416.0070181	0.92	2.23
Ala	176.91	179.32	−154.70	−154.20	162.60	164.60	179.60	−175.10	−456.5661300	−455.1810436	1.19	1.72
Phe^{g+}	176.73	−175.64	−156.20	−166.00	167.50	168.50	−175.30	−172.06	−687.6218082	−685.5021204	2.32	1.03
Phe^{a}	177.57	−178.27	−158.30	−158.50	162.30	149.90	172.44	167.61	−687.6255017	−685.5037695	0.00	0.00
Phe^{g-}	not found → converges to $\gamma_L{}^{g-}$ for both B/6+ and M/6+ levels of theory											
						γ_L						
Gly	−177.53	179.17	−82.00	−82.30	66.30	75.70	−177.95	−171.35	−417.2503687	−416.0105696	0.00	0.00
Ala	−177.52	178.94	−82.40	−82.40	74.50	80.20	−173.29	−169.55	−456.5680236	−455.1837836	0.00	0.00
Phe^{g+}	−175.49	−176.74	−81.90	−83.00	54.90	46.80	175.62	169.88	−687.6252262	−685.5037203	0.17	0.03
Phe^{a}	179.74	175.13	−82.60	−80.50	82.10	90.20	−170.75	−168.53	−687.6246985	−685.5020732	0.50	1.06
Phe^{g-}	−173.13	−167.85	−84.20	−89.10	73.40	76.30	−172.97	−170.31	−687.6249433	−685.5026585	0.35	0.70

characterized, existing force field packages could be reparametrized allowing for the evaluation of more accurate constitution- and conformer-specific MD trajectories.

Finally, the reader is encouraged to make note of the precise, modular, and explicit methodology used to define the relative spatial orientation of all constituent atomic atoms, nomenclature, and intramolecular phenomena covered in the scope of this work. As a whole, the work may be repeated at very high levels of theory, extended intramolecularly, or combined with other molecular systems to model intermolecular interactions/reactions, without the need to redefine any systemic parameter or procedure, for the 'defined NAPA portion(s)' of a larger peptide model.

The present state of theory and the physical sciences themselves cannot yet accurately and quantitatively affirm nor refute any of the conclusions proposed. The exact nature of the driving forces for and bases of energetic contributions of conformational probability, H-bond formation, and other intramolecular interactions are still largely unknown.

Acknowledgment. This work was supported by grants from the Global Institute of Computational Molecular and Materials Sciences, CEA-CNRS France (URA CNRS 2453), the National Science Foundation (NSF EPS-009190), and the NIH-BRIN grant (1 P20 RR16469). One of the authors (I.G.C.) wishes to thank the Ministry of Education for a Szent-Györgyi Visiting Professorship. The authors express their thanks and deep appreciation to Tania A. Pecora, Pablo Echenique Robba, Michelle A. Sahai, Jacqueline M. S. Law, Christopher N. J. Marai, and Benjamin Tardivel for helpful discussions and manuscript preparation. Sinisia Vukovic (GIOCOMMS, Toronto, Canada) is thanked for his help in completing the MP2 geometry optimizations at the MP2 level of theory. Professor D.-C. Fang (Beijing Normal University, China) is thanked for his helpful discussions regarding the AIM analyses. G.A.C. expresses his thanks to Emeritus Professor Alex G. Harrison (U. Toronto, Canada), Professor Alan C. Hopkinson (York U., Canada), Professor Jose-Luis Alonso (U. Zaragoza, Spain), Professor Richard F. Murphy (Creighton Medical U., USA), and Professor Julius Gy. Papp (U. of Szeged, Hungary) who continue to act as his senior mentors and 'spiritual gurus'. GIOCOMMS is further acknowledged for providing funding and support allowing this and related works to be completed in a number of international settings.

Supporting Information Available: Tables A−F. This material is available free of charge via the Internet at http://pubs.acs.org.

References and Notes

(1) Berg, M. A.; Chasse, G. A.; Deretey, E.; Füzéry, A. K.; Fung, B.; Fung, M. D. Y. K.; Henry-Riyad, H.; Lin, A. C.; Mak, M. L.; Mantas A.; Patel, M.; Repyakh, I. V.; Staikova, M.; Salpietro, S. J.; Tang, Ting-Hua.; Vank, J. C.; Perczel, A.; Csonka, G. I.; Farkas, O.; Torday, L. L.; Sze'kely, Z.; Csizmadia, I. G. *J. Mol. Struct. (THEOCHEM)* **2000**, *500*, 9.

(2) Chasse, G. A.; Rodriguez, A. M.; Mak, M. L.; Deretey, E.; Perczel, A.; Sosa, C. P.; Enriz, R. D.; Csizmadia, I. G. *J. Mol. Struct. (THEOCHEM)* **2001**, *537*, 351.

(3) Chass, G. A.; Sahai, M. A.; Law, M. S. J.; Lovas, S.; Farkas, O.; Perczel, A.; Rivail, J.; Csizmadia, I. G. *Int. J. Quantum Chem.* **2002**, *90*−*2*, 933.

(4) Sahai, A. M.; Lovas, S.; Chass, G. A.; Penke, B.; Csizmadia, I. G. *J. Mol. Struct. (THEOCHEM)* **2003**, *666*−*667*, 169.

(5) Morokuma, K.; Wipff, G. *Chem. Phys. Lett.* **1980**, *74*, 400.

(6) Steiner, R. *Acta Crystallogr.* **1998**, *D54*, 584−588.

(7) Duan, G.; Smith, V. H., Jr.; Weaver, D. F. *J. Quan. Chem.* **2000**, *80*, 44−60.

(8) Duan, G.; Smith, V. H., Jr.; Weaver, D. F. *Chem. Phys. Lett.* **1999**, *310*, 323−332.

(9) Tarakeshwar, P.; Choi, H. S.; Kim, K. S. *J. Am. Chem. Soc.* **2001**, *123*, 3323−3331.

(10) Morokuma, K. *J. Chem. Phys.* **1973**, *58*, 5823.

(11) Oki, M.; Onoda, T.; Iwamura, H. *Tetrahedron* **1968**, *24*, 1905.

(12) Vitagliano, V.; Berisio, R.; Mastrangelo, A.; Mazzarella, L.; Zagari, A. *Protein Sci.* **2001**, *10*, 2672−2632.

(13) Kitaura, K.; Morokuma, K. *Int. J. Quantum Chem.* **1976**, *10*, 325.

(14) Hirota, M.; Sekiya, T.; Abe, K.; Tashiro, H.; Karatsu, M.; Nishio, M.; Osawa, E. *Tetrahedron* **1983**, *39*, 3091.

(15) Allinger, N. L.; Flanagan, H. L. *J. Comput. Chem.* **1983**, *4*, 399.

(16) Worth, G. A.; Nardi, F.; Wade, R. C. *J. Phys. Chem. B* **1998**, *102*, 6260−6272.

(17) Chass, G. A.; Lovas, S.; Murphy, R. F.; Csizmadia, I. G. *Eur. Phys. J. D* **2002**, *20*, 481−497.

(18) Chass, G. A.; Setiadi, D. H.; Vukovic, S.; Fang, D. C.; Tang, T.-H.; Lovas, S.; Viskolcz, B.; Penke, B.; Hopkinson, A. C.; Csizmadia, I. G. *Mol. Phys.*, submitted for publication (Festschrift for Mike Robb).

(19) Wulf, O. R.; Lidde, U.; Hendericks, S. B. *J. Am. Chem. Soc.* **1936**, *58*, 2287−2293.

(20) Tamres, M. *J. Am. Chem. Soc.* **1952**, *74*, 3375−3378.

(21) Kodama, T.; Nishihata, K.; Nisho, M.; Nakagawa, N. *Tetrahedron Lett.* **1977**, 2105.

(22) Aoyama, T.; Matsuoka, O.; Nakagawa, N. *Chem. Phys. Lett.* **1979**, *67*, 508.

(23) Hobza, P.; Zahradnik, R. *Chem. Phys. Lett.* **1980**, *82* (3), 473−477.

(24) Pawliszyn, J.; Szezesniak, M. M.; Scheiner, S. *J. Phys. Chem.* **1984**, *88*, 1726.

(25) Takagi, T.; Tanaka, A.; Matsuo, S.; Maezaki, H.; Tani, M.; Fujiwara, H.; Sasaki, Y. *J. Chem. Soc.* **1987**, Perkin 2, 1015.

(26) Price, S. L.; Stone, A. J. *J. Chem. Phys.* **1987**, *86*, 2859.

(27) Waksman, G.; Kominos, D.; Robertson, S. C.; Pant, N.; Baltimore, D.; Birge, R. B.; Cowburn, D.; Hanafusa, H.; Mayer, B. J.; Overduin, M.; Resh, M. D.; Rios, C. B.; Silverman, L.; Kuriyan, J. *Nature (London)* **1992**, *358*, 646−653.

(28) Fong, T.; Cascieri, M. A.; Yu, H.; Bansal, A.; Swain, C.; Strader, C. D. *Nature (London)* **1993**, *362*, 350−353.

(29) Burkley, S. K.; Pesko, G. A. *Adv. Prot. Chem.* **1988**, 39.

(30) Armstrong, K. M.; Fairman, R.; Baldwin, R. L. *J. Mol. Biol.* **1993**, *230*, 284−291.
(31) Chakrabarti, P.; Uttamkumar, S. J. *Mol. Biol.* **1995**, *251*, 9−14.
(32) Fan M−F.; Lin, Z.; McGrady, J. E.; Mingos, D. M. P. *J. Chem. Soc.* **1996**, Perkin 2, 563.
(33) Chipot, C.; Maigret, B.; Pearlman, D. A.; Kollman, P. A. *J. Am. Chem. Soc.* **1996**, *118*, 2998−3005.
(34) McGaughey, G. B.; Gagnes, M.; Rappe A. K. π-Stacking Interactions: Alive and Well in Proteins **1998**, 273, No. 25, issue of June 19, 15458−15463.
(35) Tsuzuki, S.; Honda, K.; Uchimaru, T.; Mikami, M.; Tanabe, K. *J. Am. Chem. Soc*. **2000**, *122*, 3746−3753.
(36) Toth, G.; Murphy, R. F.; Lovas, S. *J. Am. Chem. Soc*. **2001**, *123*, 11782−11790.
(37) Toth, G.; Murphy, R. F.; Lovas, S. *Protein Eng.* **2001**, *14*, no. 8, 543−547.
(38) Steiner, T.; Koellner, G. *J. Mol. Biol.* **2001**, *305*, 535−557.
(39) Shi, Z.; Olson, C. A.; Kallenbach, N. R. *J. Am. Chem. Soc.* **2002**, *124*, 3284−3291.
(40) Chass, G. A.; Marai, C. N. J., Harrison. A. G.; Csizmadia, I. G. *J. Phys. Chem. A* **2002**, *106*, 9695−9704.
(41) Frisch, M. J.; Trucks, G. W.; Schlegel, H. B.; Scuseria, G. E.; Robb, M. A.; Cheeseman, J. R.; Zakrzewski, V. G.; Montgomery, J. A., Jr.; Stratmann, R. E.; Burant, J. C.; Dapprich, S.; Millam, J. M.; Daniels, A. D.; Kudin, K. N.; Strain, M. C.; Farkas, O.; Tomasi, J.; Barone, V.; Cossi, M.; Cammi, R.; Mennucci, B.; Pomelli, C.; Adamo, C.; Clifford, S.; Ochterski, J.; Petersson, G. A.; Ayala, P. Y.; Cui, Q.; Morokuma, K.; Malick, D. K.; Rabuck, A. D.; Raghavachari, K.; Foresman, J. B.; Cioslowski, J.; Ortiz, J. V.; Stefanov, B. B.; Liu, G.; Liashenko, A.; Piskorz, P.; Komaromi, I.; Gomperts, R.; Martin, R. L.; Fox, D. J.; Keith, T.; Al-Laham, M. A.; Peng, C. Y.; Nanayakkara, A.; Gonzalez, C.; Challacombe, M.; Gill, P. M. W.; Johnson, B. G.; Chen, W.; Wong, M. W.; Andres, J. L.; Head-Gordon, M.; Replogle, E. S.; Pople, J. A. *Gaussian 98*, revision A.11; Gaussian, Inc.: Pittsburgh, PA, 1998.
(42) Chass, G. A. *J. Mol. Struct. (THEOCHEM)* **2003**, *667*−*667*, 61.
(43) Tehrani, F. S. *Comput. Phys. Commun.* **2001**, *140*, 58.
(44) Hehre, W. J.; Radom, L.; Schleyer, P. v. R.; Pople, J. A. *Ab Initio Molecular Theory*; Wiley: New York, 1986.
(45) Roothaan, C. C. J. *Rev. Mod. Phys.* **1951**, *23*, 69.
(46) Ditchfield, R.; Hehre, W. J.; Pople, J. A. *J. Chem. Phys.* **1971**, *54*, 724.
(47) Hehre, W. J.; Ditchfield, R.; Pople, J. A. *J. Chem. Phys.* **1972**, *56*, 2257.
(48) Hariharan, P. C.; Pople, J. A. *Theor. Chim. Acta* **1973**, *28*, 213.
(49) Perczel, A.; Angyan, J. G.; Kajtar, M.; Viviani, W.; Rivail, J. L.; Marcoccia, J. F.; Csizmadia, I. G. *J. Am. Chem. Soc.* **1991**, *113*, 6256.
(50) Almeida, D. R. P.; Pisterzi, L. F.; Chass, G. A.; Torday, L. L.; Varro; Papp, J. Gy.; Csizmadia, I. G. *J. Phys. Chem. A* **2002**, *106* (43), 10423−10436.
(51) Pisterzi, L. F.; Almeida, D. R. P.; Chass, G. A.; Torday, L. L.; Varro; Papp, J. Gy.; Csizmadia, I. G. *Chem. Phys. Lett.* **2002**, *365*, 542−551.
(52) Bombasaro, J. A.; Suvire, F. D.; Chasse, G. A.; Zamarbide, G. N.; Estrada, M. R. *J. Mol. Struct. (THEOCHEM)* **2001**, *548*, 39−46.
(53) Villagra, S. E.; Santillian, M. B.; Rodriguez, A. M.; Chasse, G. A.; Freile, M. L.; Zacchino, S.; Enriz, R. D.; Matyus, P. *J. Mol. Struct. (THEOCHEM)* **2001**, *549*, 217−228.
(54) Head-Gordon, M.; Pople, J. A.; Frisch, M. J. *Chem. Phys. Lett.* **1988**, *153*, 503.
(55) Scoot, A. P.; Radom, L. *J. Phys. Chem.* **1996**, *100*, 16502.
(56) Becke, A. D. *Phys. Rev. A* **1988**, *38*, 3098.
(57) Lee, C.; Yang, W.; Parr, R. G. *Phys. Rev. B* **1988**, *37*, 785.
(58) Becke, A. D. *J. Chem. Phys.* **1993**, *98*, 5648.
(59) Scott, A. P.; Radom, L. *J. Phys. Chem.* **1996**, *100*, 16502.
(60) Bader, R. F. W. *Atoms in Molecules. A Quantum Theory*; Clarendon Press: Oxford, 1990; *Angew. Chem., Int. Ed. Engl.* **1994**, *33*, 620.
(61) Bader, R. E. W.; Biegler-König, F. W.; Cheeseman, J. R.; Duke, J. A.; Keith, T. A.; Krug, P.; Laidig, K. E.; Langdon, B. *AIMPAC* (a set of programs for the theory of atoms in molecules); McMaster University: Hamilton, ON, Canada, 1994. Biegler-König, F. W.; Bader, R. F. W.; Tang, T.-H. *J. Comput. Chem.* **1982**, *3*, 317−328.
(62) Fang, D.-C., Tang, T.-H. *AIM98PC* (a modified PC version of *AIMPAC*); Beijing Normal University: Beijing, China, 1998.
(63) Biegler-König, F. W.; Schönbohn, J.; Bayles, D. *J. Comput. Chem.* **2002**, *22*, 545−559. Biegler-König, F. W.; Schönbohn, J. *J. Comput. Chem.* **2002**, *23*, 1489−1494.
(64) Møller, C.; Plesset, M. S. *Phys. Rev.* **1934**, *46*, 618.
(65) Molekel: Flükiger, P. F. Development of the molecular graphics package MOLEKEL and its application to selected problems in organic and organometallic chemistry, Thèse No 2561, Département de chimie physique, Université de Genève, Genève, 1992.
(66) Portman, S.; Lüthi, H. P. MOLEKEL: An Interactive Molecular Graphics Tool. *Chimia* **2000**, *54*, 766−770.
(67) MacDiarmid, A. G. *Rev. Mod. Phys.* **2001**, *73*, 701.
(68) Ozaki, M.; Takahashi, A. *Chem. Phys. Lett.* **1986**, *127*, 242.
(69) Newton, M. D.; Stanton, R. E. *J. Am. Chem. Soc.* **1986**, *108*, 2469.
(70) Lothi, H. P.; Alml, F. J. *Chem. Phys. Lett.* **1987**, *135*, 357.
(71) Nelson, D.; Perng, T. *Proc. Oklahoma Acad. Sci.* **2000**, *80*, 141.
(72) Chin, W.; Mons, M.; Dognon, J.-P.; Mirasol, R. S.; Chass, G.; Dimicoli, I.; Piuzzi, F.; Butz, P.; Tardivel, B.; Compagnon, I.; von Helden, G.; Meijer, G. *J. Phys. Chem A* **2005**, *109*, 5281.